NASA Tech Briefs

National Aeronautics and
Space Administration

Electronic Components and Circuits

Electronic Systems

Physical Sciences

Materials

Computer Programs

Mechanics

Machinery

Fabrication Technology

Mathematics and Information Sciences

Life Sciences

98-04

April 1998

INTRODUCTION

Tech Briefs are short announcements of new technology derived from the research and development activities of the National Aeronautics and Space Administration. These Briefs emphasize information considered likely to be transferable across industrial, regional, or disciplinary lines and are issued to encourage commercial application.

Availability of NASA Tech Briefs and TSP's

Distribution of NASA Tech Briefs, a monthly periodical publication, is limited to engineers in U.S. Industry and to other domestic technology transfer agents. Requests for individual Tech Briefs or for Technical Support Packages (TSP's) announced herein should be addressed to

NASA Center for AeroSpace Information
Technology Transfer Office
800 Elkridge Landing Rd.
Linthicum Heights, MD 21090-2934
Telephone No. (301) 621-0245

Please reference the three-letter, five-digit control number located at the end of each Tech Brief. Information on NASA's Technology Utilization Program, its documents, and services is also available at the same facility.

Technology Utilization Officers and Patent Counsels are located at NASA field installations to provide technology-transfer access to industrial users. Inquiries can be made by writing to NASA field installations listed below.

Technology Utilization Officers and Patent Counsels

Ames Research Center
Technology Utilization Officer
Mail Code 223-3
Moffett Field, CA 94035

Patent Counsel
Mail Code 200-11
Moffett Field, CA 94035

Goddard Space Flight Center
Technology Utilization Officer
Mail Code 702-1
Greenbelt, MD 20771

Patent Counsel
Mail Code 204
Greenbelt, MD 20771

Lyndon B. Johnson Space Center
Technology Utilization Officer
Mail Code IC-4
Houston, TX 77058

Patent Counsel
Mail Code AL3
Houston, TX 77058

John F. Kennedy Space Center
Technology Utilization Officer
Mail Stop PT-PMO-A
Kennedy Space Center, FL 32899

Patent Counsel
Mail Code PT-PAT
Kennedy Space Center, FL 32899

Langley Research Center
Technology Utilization Officer
Mail Stop 143
Hampton, VA 23665

Patent Counsel
Mail Code 279
Hampton, VA 23665

Lewis Research Center
Technology Utilization Officer
Mail Stop 7-3
21000 Brookpark Road
Cleveland, OH 44135

Patent Counsel
Mail Code LE-LAW
21000 Brookpark Road
Cleveland, OH 44135

Jet Propulsion Laboratory
Technology Utilization Officer
Mail Stop 156-211
4800 Oak Grove Drive
Pasadena, CA 91109

NASA Resident Office-JPL
Technology Utilization Officer
Mail Stop 180-801
4800 Oak Grove Drive
Pasadena, CA 91109

Patent Counsel
Mail Code 180-801
4800 Oak Grove Drive
Pasadena, CA 91109

George C. Marshall Space Flight Center
Technology Utilization Officer
Code AT01
Marshall Space Flight Center, AL 35812

Patent Counsel
Mail Code CC01
Marshall Space Flight Center, AL 35812

John C. Stennis Space Center
Technology Utilization Officer
Code HA-30
Stennis Space Center, MS 39529

NASA Headquarters
Technology Utilization Officer
Code CU
Washington, DC 20546

Assistant General Counsel for Patent Matters
Code GP
Washington, DC 20546

Dryden Flight Research Center
Technology Utilization Officer
M/S D21-31
Bldg. 4832 Whse 7
Lilly Dr.
Edwards, CA 93523

BLANK PAGE

NASA TechBriefs

National Aeronautics and
Space Administration

April 1998
98-04

BLANK PAGE

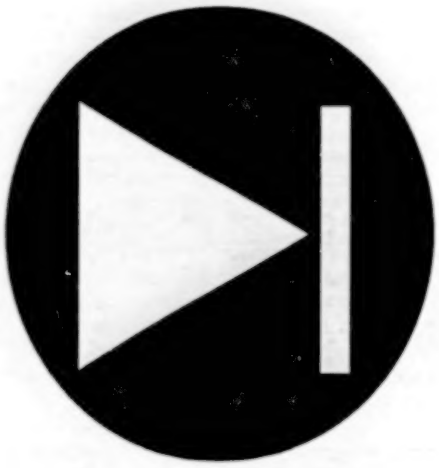

Electronic Components and Circuits

Hardware, Techniques, and Processes

BLANK PAGE

Computation of Characteristics of a Helical TWT Slow-Wave Circuit

Accurate numerical simulation can be substituted for experimentation to reduce the cost of development.

Lewis Research Center, Cleveland, Ohio

A computational study has been performed to show that one can accurately compute the cold-test electromagnetic characteristics of the helical slow-wave circuit of a traveling-wave tube (TWT).

Previous efforts to apply computer-aided design techniques to helical TWT circuits had involved computer codes based partly on simplifying approximations of TWT geometries as they relate to electromagnetic characteristics; helices have been approximated as sheaths, helix tapes have been approximated as having zero thicknesses, and dielectric rods that support the helices have been approximated by combinations of homogeneously and inhomogeneously loaded volumes with effective permittivities. However, to simulate electromagnetic characteristics accurately, one must use a computer code that represents the geometry of the TWT in its three-dimensional complexity. This can be done by use of the computer program MAFIA (Solution of **Ma**xwell's Equations by the **F**inite-**I**ntegration-**A**lgorithm) — a powerful, modular electromagnetic-simulation code written in FORTRAN 77 for use in the computer-aided design and analysis of two- and three-dimensional electromagnetic devices, including magnets, radio-frequency cavities, waveguides, and antennas.

In MAFIA, the geometric accuracy is limited only by the resolution of the computational grid used to represent the geometry of the modeled device. The finite integration technique (FIT) algorithm implemented in MAFIA yields a matrix of finite-difference equations for the electric and magnetic fields in the device under study. Solutions can be obtained in the time or the frequency domain, or in the static domain where applicable.

In the study, MAFIA was applied to a TWT slow-wave structure that included a copper-plated rectangular tape wound into a helix, which was supported by rectangular BeO dielectric rods inside a conductive barrel (see Figure 1). The electrical resistivities of the helix and barrel; the width, thickness, and helical pitch of the tape; and the dielectric properties and dimensions of the rods were all incorporated into the MAFIA model.

The TWT cold-test characteristics of primary interest are the slow-wave dispersion (normalized phase velocity vs. frequency), the on-axis electron-beam/slow-wave interaction impedance, and radio-frequency (RF) losses. The computational approach to determining the dispersion characteristics involved the use of boundary conditions analogous to those used in the experimental approach: In the experimental approach, one determines the dispersion characteristics from measurement of resonant frequencies of a section of the slow-wave circuit shorted at both longitudinal ends. In the computational approach, a MAFIA helix model is truncated with either electric or magnetic walls at two end points to simulate standing waves with an integral number of half wavelengths in the circuit section thus isolated.

The interaction impedance is computed directly by calculating the magnitude of the space harmonic component of the longitudinal electric field with which the electron beam is synchronous, and the total RF power flow. Because the interaction impedance cannot be measured directly, the experimental approach involves measuring resonant frequencies in a perturbed resonant circuit and deriving an expression relating the change in resonant frequen-

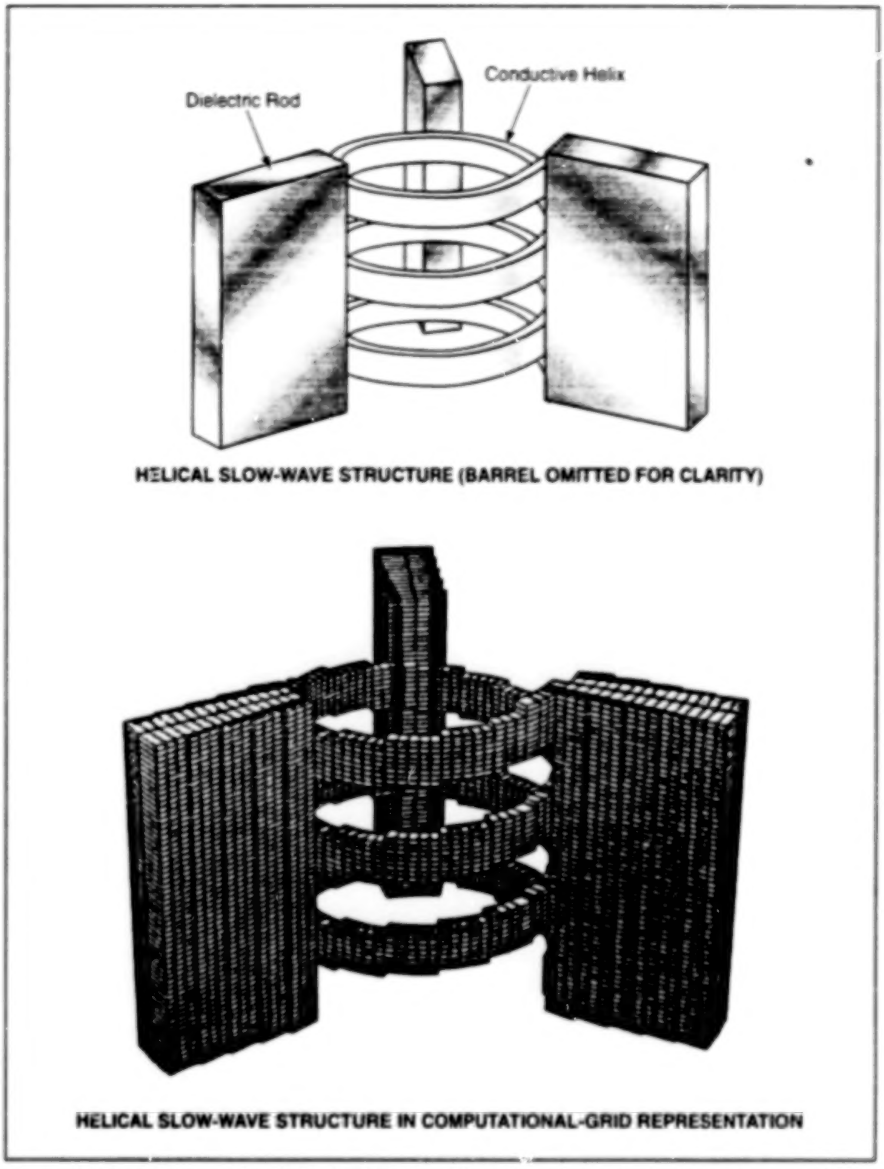

Figure 1. **Three Turns of the Helical TWT Slow-Wave Circuit** are depicted here by a plot from MAFIA, wherein the helix is generated in a cylindrical coordinate system by varying axial and azimuthal coordinates consistently with the formula for a circular helix. For clarity, the barrel surrounding the dielectric rods is omitted from this view.

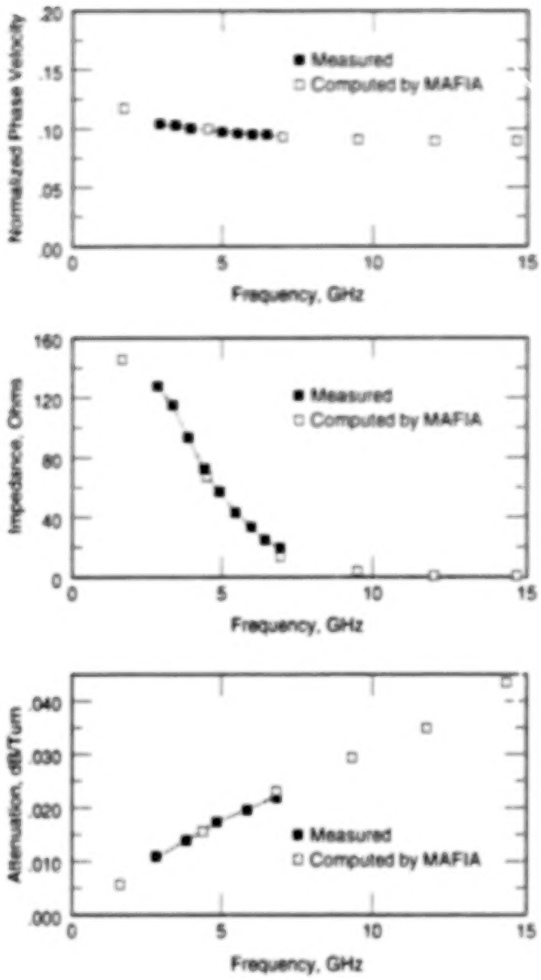

Figure 2. **Three Parameters of Major Interest** for characterizing the performance of the slow-wave structure depicted in Figure 1 were computed by MAFIA and measured.

cies between the perturbed and unperturbed circuits to the interaction impedance. This derivation necessitates several approximations, rendering the experimental procedure less accurate than direct computation with MAFIA.

The computation of RF losses involves consideration of the effects of finite conductivity of the helix and barrel, and of the loss tangent of the dielectric (taken to be 0.0006 for BeO). In the study, the effect of surface roughness in increasing the effective resistivity of the tape was also taken into account. The total RF loss was calculated as a sum of surface resistivity and dielectric losses and summarized in terms of attenuation per turn of the helix as a function of frequency.

Figure 2 shows principal electromagnetic parameters of the slow-wave structure, both as computed by MAFIA and as determined experimentally. The excellent agreement between computational and experimental results demonstrates the utility of numerical simulation as a substitute for building and testing TWTs to analyze numerous alternative TWT designs. In comparison with experimentation, numerical simulation costs less and takes less time, and thereby also affords additional freedom to analyze both novel designs and small variations on previous designs.

This work was done by Carol L. Kory of Analex Corp. for **Lewis Research Center**. *Further information is contained in a TSP [see page 1].*

Inquiries concerning rights for the commercial use of this invention should be addressed to NASA Lewis Research Center, Commercial Technology Office, Attn: Tech Brief Patent Status, Mail Stop 7-3, 21000 Brookpark Road, Cleveland, Ohio 44135. Refer to LEW-16571.

Line-Focus Photovoltaic Module With Solid Secondary Optics

Cell design and optical and electrical configurations are combined to obtain high efficiency.

Lewis Research Center, Cleveland, Ohio

The figure illustrates aspects of a lightweight, relatively inexpensive solar photovoltaic module suitable for use on Earth or in outer space in conjunction with at least a single-axis Sun-tracking apparatus. The module contains line-focus primary Fresnel lenses that act in conjunction with spot-focus, compound parabolic secondary solid optics to concentrate incident sunlight onto tandem, paired GaAs and GaSb photovoltaic cells arrayed along the focal lines. The tandem-photovoltaic-cell design and the optical and electrical configurations are combined to obtain high energy-conversion efficiency. In addition, the incorporation of the secondary solid optics increases resistance to ionizing radiation.

Each line-focus (cylindrical) Fresnel lens comprises a thin, arched glass superstrate sheet that protects and supports a silicone rubber sheet, into which Fresnel-lens grooves have been molded. A spot-focus secondary solid optic is adhesively bonded to the input face of each tandem GaAs/GaSb cell pair. Each secondary optic, molded in silicone rubber, features rectangular entrance and exit apertures with parabolic side walls, on which incident light is totally internally reflected. The parameters of the parabolas are chosen in conjunction with the length and width of the tandem cell pair to maximize the concentration of light onto the cells over suitable acceptance and Sun-pointing-error angles. Taking advantage of the rectangularity of the entrance aperture, each secondary optic can be butted up against the adjacent secondary optic(s) to maximize utilization of the light focused by the Fresnel lens.

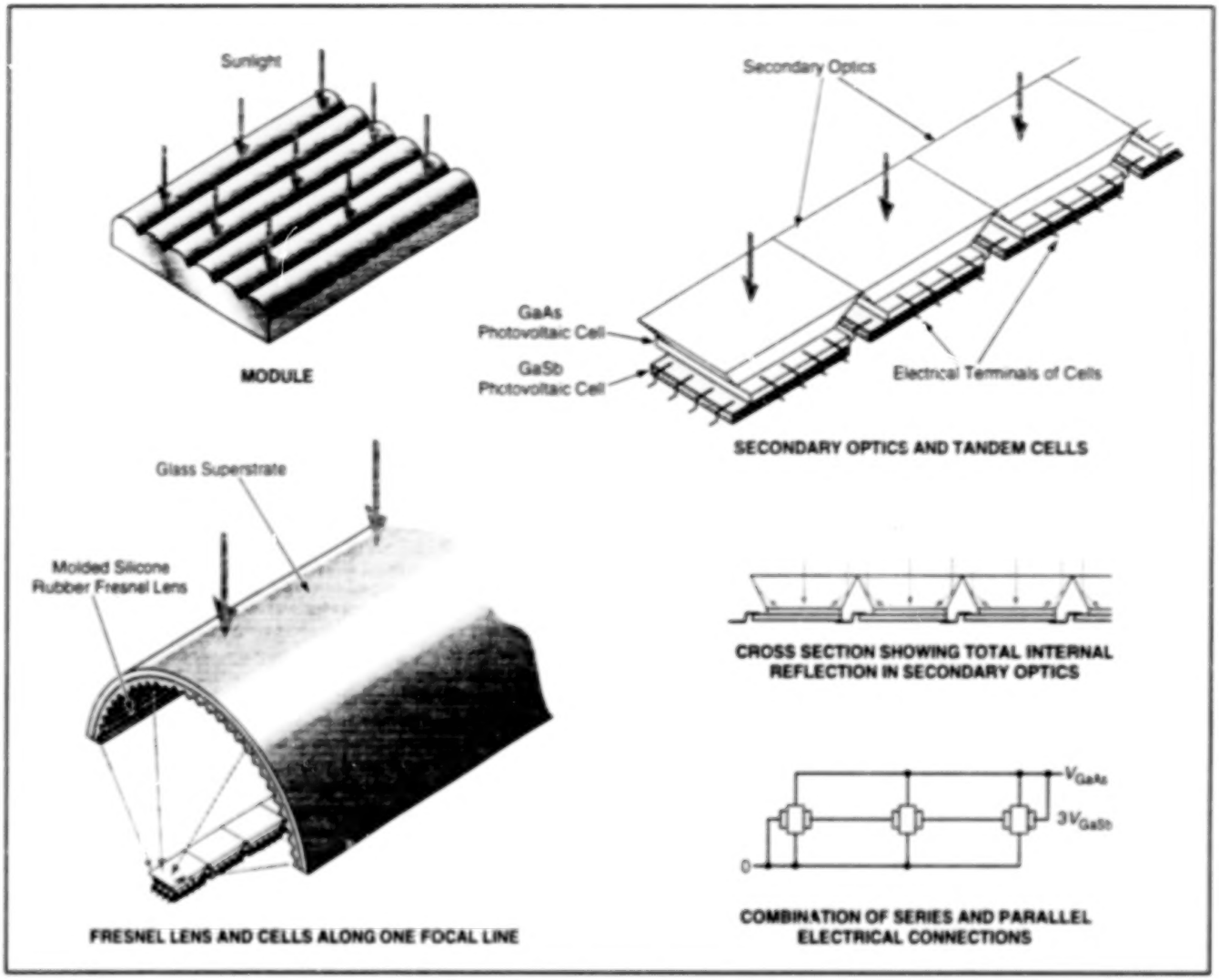

Fresnel Lenses and Secondary Optics are used together to concentrate light more effectively than could be done using either type of optic alone. The overall design affords enhanced energy-conversion efficiency.

The tandem pairs of cells are designed to enhance energy-conversion efficiency by exploiting differing spectral sensitivities. The top (GaAs) cell in each pair is sensitive to the visible portion of sunlight and allows the infrared portion to pass through to the bottom (GaSb) cell, which is sensitive to infrared. The energy-conversion efficiency of the GaAs cell is 24 percent, while that of the GaSb cell is 6 percent; thus, the energy-conversion efficiency of the tandem cell pair is 30 percent.

The terminals of the tandem cells in each pair are arranged perpendicularly to each other. Tandem-cell pairs are grouped together in threes along each focal line, by use of a voltage matching combination of series and parallel electrical connections: Each GaSb cell generates one-third the voltage of a GaAs cell. The GaSb cells in each triplet are connected in series along the focal line, while the GaAs cells in each triplet are connected in parallel. Thus, the voltage of the triplet series of GaSb cells matches the voltage of the GaAs cells, making it possible to connect both triplets in parallel. All of the series/parallel connected triplets along the focal line can then be strung together in series to obtain a higher output voltage.

The cells are mounted on ceramic substrates (omitted from the figure for clarity). The series and parallel electrical connections are formed in metal patterns on the substrates. Because the series connections are made over short distances along the focal lines, the overall series electrical resistance is relatively low.

A prototype module containing 24 tandem-cell pairs was constructed and tested under simulated sunlight in the absence of the atmosphere. The overall output of the module amounted to an average power of 2.61 W per cell — corresponding to an overall energy-conversion efficiency of 23.3 percent. In contrast, the energy-conversion efficiencies of relatively expensive, fragile, large-area arrays of flat Si and GaAs cells have generally been less than 20 percent.

This work was done by Lewis M. Fraas and James E. Avery of JX Crystals, Inc., and Mark J. O'Neill of Entech, Inc., for **Lewis Research Center**. *Further information is contained in a TSP [see page 1].*

Inquiries concerning rights for the commercial use of this invention should be addressed to NASA Lewis Research Center, Commercial Technology Office, Attn: Tech Brief Patent Status, Mail Stop 7-3, 21000 Brookpark Road, Cleveland, Ohio 44135. Refer to LEW-16385.

Pulse Shepherding in Nonlinear Fiber Optics

Copropagating pulses at different wavelengths can be maintained in alignment.

NASA's Jet Propulsion Laboratory, Pasadena, California

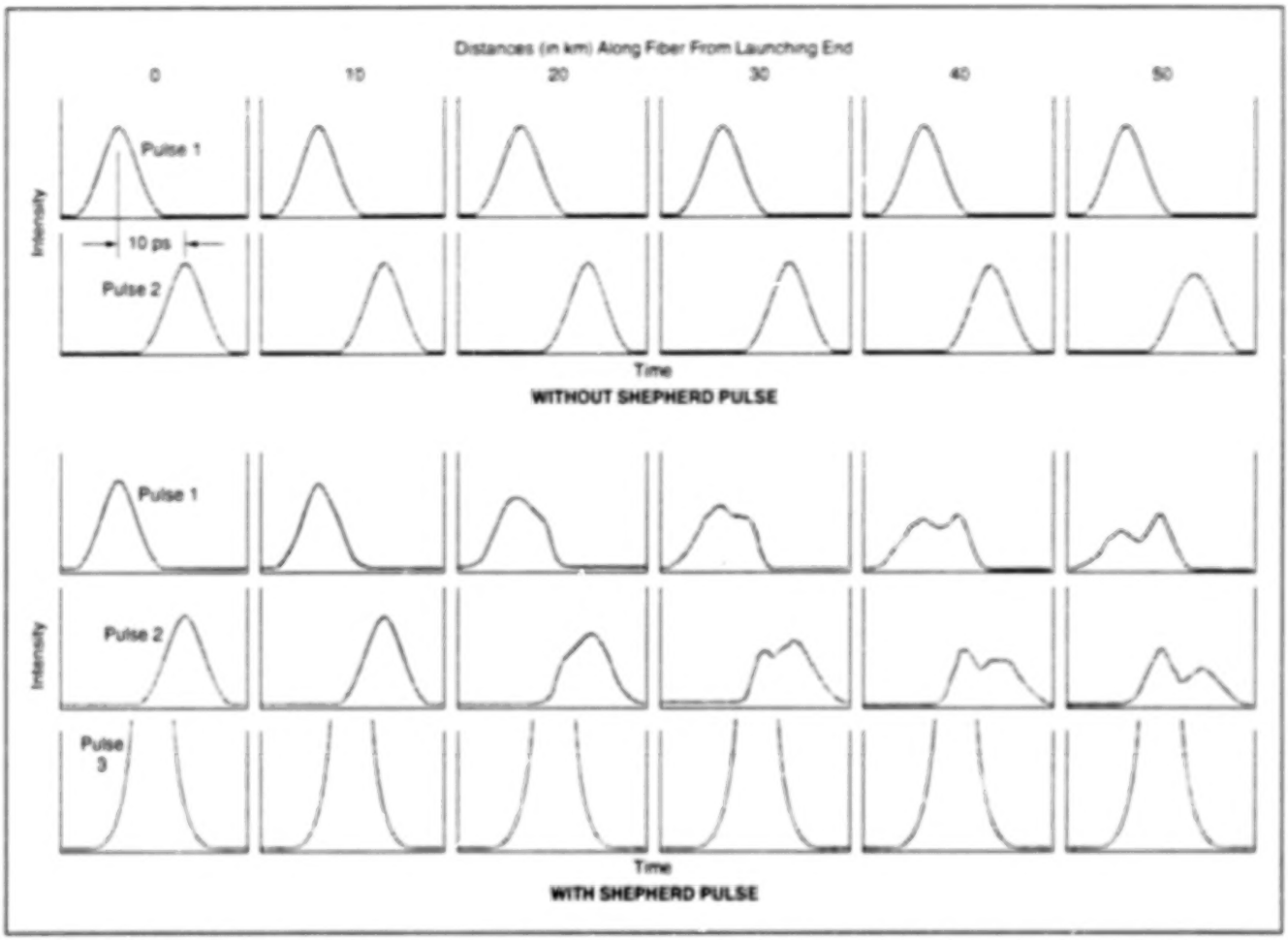

Waveforms of Pulses at various positions along the optical fiber illustrate the effect of pulse 3 (the shepherd pulse) on the evolution of pulses 1 and 2. After propagating 50 km along the fiber, parts of pulses 1 and 2 become aligned with (in effect, "herded" by) the shepherd pulse.

Pulse shepherding is a nonlinear signal-propagation phenomenon that can occur when several pulses of light at different wavelengths are launched simultaneously or nearly simultaneously along the same single-mode optical fiber under suitable conditions. As its name suggests, pulse shepherding involves the use of one pulse (denoted the shepherd pulse) to "herd" together a number of other pulses that propagate along with it.

Pulse shepherding could likely be exploited to ensure the simultaneity of arrival of pulses at different wavelengths that represent parallel bits of data in a wavelength-division-multiplexing digital communication system — in other words, to "herd" together the bit pulses of each byte. Without pulse shepherding, wavelength dispersion in the fiber material causes pulses traveling at different wavelengths to arrive at somewhat different times; in a high-speed digital system with a long optical fiber, differences between times of arrival can become excessive relative to the byte period.

Discovered through theoretical analysis and computer simulation, pulse shepherding involves cross phase modulation, which is an unavoidable interaction between copropagating pulses that arises from nonlinearity in the response of the fiber-optic material. In cross phase modulation, copropagating pulses affect each other through the intensity dependence of the index of refraction. Cross phase modulation does not cause exchange of energy among the pulses, but it does affect the shapes and relative locations of the pulses. In designing for pulse shepherding, one designs the optical fiber to eliminate group-velocity mismatches among the wavelength channels and selects the timing, amplitudes, and shapes of the pulses in the various wavelength channels to exploit cross modulation to bring and keep the pulses together as they propagate.

In the theoretical analysis, the copropagation of M pulses is modeled by M simultaneous, coupled, nonlinear equations. The solution is generated numerically by the split-step Fourier method, which involves a forward-stepping process in which the solution is first advanced using only the nonlinear parts of the equations, then advanced using only the linear parts of the equations. The Fourier transform in this method is generated by the fast-Fourier-transform technique.

The figure illustrates the results of these computations for an example of two Gaussian-shaped pulses of 10-ps duration, propagating both without and with a third (shepherd) pulse along a suitably designed optical fiber 50 km long. In this example, pulse 1 at a wavelength of

1.550 μm is launched at one pulse duration before pulse 2 at a wavelength of 1.546 μm. In the absence of a shepherd pulse, the pulses 1 and 2 remain separated throughout their travel. When pulse 3 (the shepherd pulse) at a wavelength of 1.542 μm and at twice the amplitude of pulses 1 and 2 is launched midway between pulses 1 and 2, the three pulses become increasingly aligned with each other as they travel along the fiber. It is as though the shepherd pulse were pulling backward on the leading pulse and pulling forward on the trailing pulse.

The figure also illustrates another interesting phenomenon: if one uses too strong a shepherd pulse in an attempt to pull pulses 1 and 2 together sooner, one may not succeed. Instead, pulses 1 and 2 could be broken up, with one part of each pulse becoming shepherded and the remainder continuing to propagate by itself.

This work was done by Larry Bergman and Cavour Yeh of Caltech for **NASA's Jet Propulsion Laboratory**. *Further information is contained in a TSP [see page 1].*

In accordance with Public Law 96-517, the contractor has elected to retain title to this invention. Inquiries concerning rights for its commercial use should be addressed to

Technology Reporting Office
JPL
Mail Stop 122-116
4800 Oak Grove Drive
Pasadena, CA 91109
(818) 354-2240

Refer to NPO-19987, volume and number of this NASA Tech Briefs *issue, and the page number.*

Discriminator-Stabilized Superconductive/Ferroelectric Oscillator

Phase noise can be made less than that of a frequency-multiplied crystal oscillator.

Lewis Research Center, Cleveland, Ohio

An oscillator circuit that contains superconductive and ferroelectric resonator elements is undergoing development. This circuit is designed to serve as a frequency-locked local oscillator in a communication system in which digital data are conveyed via phase modulation on a carrier signal, the frequency of which could be as high as tens of gigahertz.

The traditional practice of multiplying the frequency of a crystal-stabilized oscillator is not suitable in this application because of phase noise. The highest practical crystal frequency is a few hundred megahertz, and the phase noise is proportional to the square of the frequency-multiplication factor, N. At the large N necessary for reaching tens of gigahertz, the phase noise is large enough to contribute significantly to the bit-error rate. The developmental circuit oscillates directly at the desired frequency, obviating the phase-noise multiplication. Although a dielectric disk oscillator could operate in the desired frequency range, it also generates excessive phase noise and cannot be electronically tuned or locked in frequency. The developmental circuit can be electrically tuned and can be electronically locked in frequency, with a concomitant reduction in phase noise.

The heart of the oscillator is a pseudomorphic high-electron-mobility transistor (PHEMT) connected to a microstrip ring resonator with integral coupled lines (see figure). The coupled lines are formed from a thin film of a high-temperature superconductor (HTS) over a thin film of a ferroelectric material like $Ba_xSr_{1-x}TiO_3$ (where $0 \leq x \leq 1$). The combination of the HTS and the ferroelectric material is chosen to obtain the high resonance quality factor (Q) needed for low phase noise (phase noise is proportional to Q^{-3}).

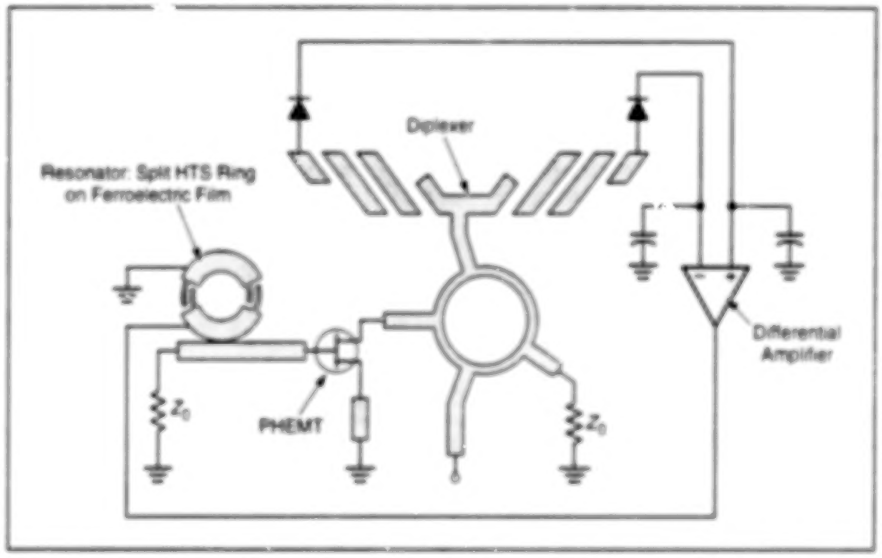

This Oscillator Circuit is designed to generate a frequency-stabilized signal with phase noise low enough for high-order phase-modulation formats.

The coupled lines are designed so that most of the electromagnetic energy is confined in the odd mode of propagation, in which the electric field is concentrated in the dielectric (that is, the ferroelectric) material. Tuning is effected by applying a dc bias voltage to alter the permittivity of the ferroelectric material. To enhance tuning, the coupled lines are positioned at radio-frequency voltage maxima along the ring. To diminish loading, the dc-bias connections are made at radio-frequency voltage minima along the ring.

The output of the oscillator is fed into a hybrid ring or directional coupler to enable sampling of the output. The sampled power is fed into a diplexer, the crossover frequency of which equals the desired frequency of oscillation. The high- and low-pass outputs of the diplexer are detected by diodes, then low-pass filtered to remove radio-frequency components. The resulting dc signals are applied to the input terminals of a differential operational amplifier. The differential amplifier puts out a dc voltage that is superimposed upon a fixed offset voltage, and the resulting total voltage constitutes the dc bias applied to the resonator ring. (For the sake of clarity, the circuit is depicted in simplified form in the figure, without the components for generating the fixed offset voltage and superimposing the amplifier output.)

If the actual frequency of oscillation is greater (or less) than the crossover frequency, then the diplexer generates a

high-pass (or low-pass) output, causing the differential amplifier to decrease (or increase) the dc bias. This action causes the permittivity of the ferroelectric material to increase (or decrease) thereby causing the frequency of oscillation to decrease (or increase). In other words, the dc bias is adjusted to correct for any deviation from the crossover frequency.

Alternatively, if frequency stability is not of concern, one can simply adjust the bias voltage directly to effect tuning. For example, a sawtooth or other suitable waveform could be applied to obtain a repetitive frequency sweep.

This work was done by Robert R. Romanofsky and Felix A. Miranda of **Lewis Research Center**. *Further information is contained in a TSP [see page 1].*

Inquiries concerning rights for the commercial use of this invention should be addressed to NASA Lewis Research Center, Commercial Technology Office, Attn: Tech Brief Patent Status, Mail Stop 7-3, 21000 Brookpark Road, Cleveland, Ohio 44135. Refer to LEW-16440.

Glove Senses Angles of Finger Joints

Resistances of conductive elastomeric strips change with stretching.

Lyndon B. Johnson Space Center, Houston, Texas

A glove has been instrumented to sense the angles of finger joints via the electrical resistances of strips of an electrically conductive elastomer on the backs of the fingers, including the thumb (see figure). The conductive elastomer is a urethane-based synthetic rubber filled with conductive carbon particles.

One end of each conductive elastomeric strip is connected to the tip of a digit through an elastic band. The other end of the strip is attached to the base of the digit through another elastic band. Each conductive elastomeric strip is routed through a plastic cylinder (not shown in the figure) that prevents the strip from rolling off the back side of the affected digit when the digit is bending.

The electrical resistance of each strip decreases when the strip is stretched by increased bending of the joints on the digit. Wires connect the ends of the strips to simple instrumentation amplifiers. The outputs of these amplifiers are voltages indicative of the resistances of the strips and thus the angles of the joints.

The glove is a prototype of a sensor apparatus for providing hand-configuration feedback for an interactive virtual-reality or other display system. In comparison with other instrumented gloves and glovelike exoskeletal devices developed previously for the same purpose, this glove costs much less. Elastomeric sensors based on the same principle might also be used to measure bending of arm and leg joints and to measure stretching and bending of other body parts.

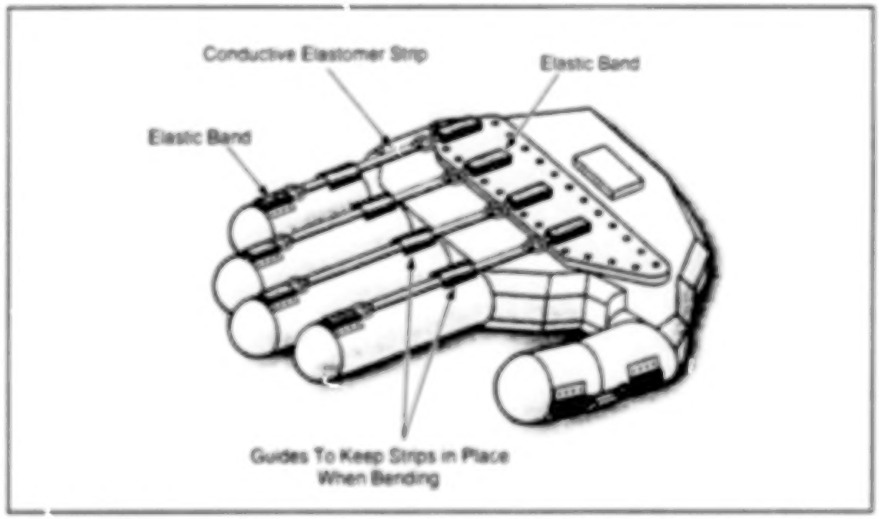

Conductive Elastomeric Strips are stretched by bending of finger joints, with consequent changes in their electrical resistances.

This work was done by Larry C. Li, Fredric Dawn, and Todd A. Pesek of **Johnson Space Center**. *Further information is contained in a TSP [see page 1].*

This invention is owned by NASA, and a patent application has been filed. Inquiries concerning nonexclusive or exclusive license for its commercial development should be addressed to the Patent Counsel, Johnson Space Center [see page 1]. Refer to MSC-22513.

Computing Limiting Voltages vs. Temperatures for Ni/Cd Cells

Mathematical modeling replaces experimentation to some extent.

NASA's Jet Propulsion Laboratory, Pasadena, California

Curves of limiting voltage (*V*) as a function of temperature (*T*) for nickel/cadmium cells and batteries can be computed by use of a mathematical cell model based on first principles. Such curves ("V/T curves" for short) are needed as guides to rapid full charging without overcharging. Charge-control techniques based on V/T curves are being developed for Ni/Cd cells aboard spacecraft in low orbits around the Earth. These techniques could also be used on Earth; for example, to control the charging of Ni/Cd batteries in electric vehicles during regenerative braking.

Full charging of a Ni/Cd cell is necessary for maintaining its charge capacity. Because a Ni/Cd cell exhibits a negative temperature coefficient of voltage, it can go into a thermal-runaway condition when it becomes heated during overcharging, especially if overcharging occurs at a high current. Even when unaccompanied by thermal runaway, overcharging can degrade the cell and shorten its life. Thus, it is necessary to prevent overcharging as well as undercharging. The relevant measure of charge

is the charge in ÷ charge out; it is denoted as the recharge fraction, the charge/discharge ratio, or the reciprocal of the cell throughput efficiency. The minimum value of this measure to ensure full charging is somewhat greater than 1, and the maximum allowable value to prevent damage is higher. V/T curves are chosen so that by adhering to them, one can achieve the desired recharge fraction between the minimum and maximum values at a given temperature in a relatively wide temperature range.

Heretofore, it has been necessary to construct V/T curves from experimental data. However, experiments to determine V/T curves for Ni/Cd cells and batteries are tedious and destructive. Moreover, the interpretation of experimental data involves uncertainties in that the characteristics of Ni/Cd cells depend partly on prior thermal and charge/discharge histories. Thus, there is a need for the present method of estimating V/T curves without having to perform experiments.

The mathematical model used in the present method is built around the following principles of:

- Material balance for the dissolved chemical species generated and consumed in electrochemical reactions and transported by diffusion and migration,
- Changes in electrochemical potential in the solid phase and in the electrolyte,
- Charge-transfer kinetics as represented by a modified Butler-Volmer rate equation,
- Conservation of charge in the electrochemical cell, and
- Effects of intercalation and slow diffusion of protons into the positive electrode.

This model involves a simplification from porous-electrode models in that mass-transport processes in the solid phase are recognized as predominating over those in the liquid phase and thus a uniform reaction layer on a planar electrode is assumed. The model can be used to predict the charge/discharge characteristics of a cell under any specified test conditions, including typical conditions like constant current, constant voltage, or constant power, with limits of time, voltage, current, or temperature. The model also accounts for the existence of two forms (the β and γ phases) of the positive active material (NiOOH) and the corresponding reduced forms [the β and α phases of $Ni(OH)_2$] to provide a more accurate prediction of discharging and charging behavior.

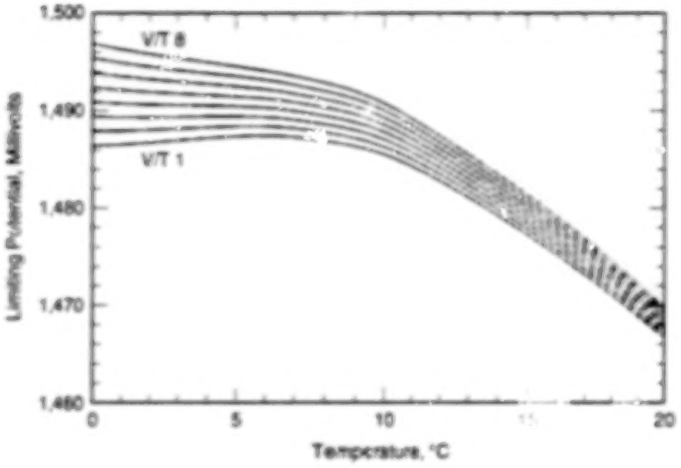

Each of the Eight Curves represents the voltage, as a function of temperature, corresponding to one of eight values of percent recharge between the minimum and maximum allowed values. These curves were computed from a mathematical model of the charge/discharge characteristics of a rechargeable Ni/Cd electrochemical cell.

The figure presents a set of V/T curves computed by use of the model for a Ni/Cd cell under typical repetitive low-Earth-orbit charge/discharge cycling. These curves are shaped similar to experimentally determined V/T curves. In comparison with experimental curves, the curves give slightly reduced percent recharge at a given voltage or slightly higher voltage for a given percent recharge, less sensitivity to changes in inrush current, and less voltage span corresponding to the desired range of percent recharge. These differences are being addressed in continuing research.

This work was done by Ratnakumar Bugga, Paul Timmerman, and Sal DiStefano of Caltech for **NASA's Jet Propulsion Laboratory**. *Further information is contained in a TSP [see page 1].*

NPO-20152

BLANK PAGE

Electronic Systems

Hardware, Techniques, and Processes

BLANK PAGE

Lightning Detection and Ranging System

This system provides relatively comprehensive indications of lightning activity in the vicinity.

John F. Kennedy Space Center, Florida

The Lightning Detection and Ranging (LDAR) system is a network of lightning-monitoring stations at Kennedy Space Center. The LDAR system contains equipment for measuring and indicating the three-dimensional locations and times of lightning flashes that have occurred within distances up to tens of kilometers. The LDAR system enables weather forecasters to give timely warnings of imminent lightning hazards that can affect local outdoor activities, and to terminate the warnings with confidence when lightning no longer poses a danger.

The LDAR system includes seven stations: a central observing/controlling/computing station and six remote observing stations in a somewhat irregular hexagonal pattern (see figure). The remote observing stations are approximately 8 km distant from the central station. Each observing station continuously detects radiation in a frequency band centered at 66 MHz and amplifies the detected signal enabling the system to handle signals with the wide dynamic range typical of those from lightning.

The position from which a signal originated (the presumed location of the lightning flash) can be computed from the speed of light, the differences among the times of arrival of the signals, and the known positions of the stations. The speed of LDAR system electronics allows timing resolution as fine as 10 ns. Measurements from the central station and three remote stations are necessary for this computation. Because the system contains six remote stations, the system consists, in effect, of two subsystems, one of which can be regarded as redundant. The resulting overdeterminacy in the data provides indications of the quality of the data: if locations of the same lightning flash computed from different nonredundant subsets of the data are acceptably close to each other, then an average of the locations is accepted and displayed; otherwise, the data from the particular lightning flash are regarded as unreliable and the location is not displayed.

The LDAR system offers numerous advantages over other lightning-monitoring systems, both governmental and commercial. One advantage is sensitivity: Whereas most other systems locate only cloud-to-ground lightning, the LDAR system detects and locates essentially all lightning, including inter- and intracloud strokes. As a result, the LDAR system detects lightning at least as early as other systems do (sometimes 10 to 20 min earlier), thereby providing greater warning lead times. Also, because the LDAR system detects more of the lightning activity, forecasters can have greater confidence in terminating warnings, sometimes as much as an hour earlier than would be necessary when using other lightning-monitoring systems.

The LDAR system also provides more comprehensive information on the evolving three-dimensional distribution of lightning activity in the vicinity. A typical commercial system locates one point per flash or return stroke, whereas for one flash, the LDAR system locates an average of about 200 points, covering an average ground area of 11.4 km^2. Commercial lightning-monitoring systems generally provide only two-dimensional location data with errors of the order of 2 km, whereas the LDAR provides radarlike three-dimensional location data with errors of 150 m.

The LDAR information creates heretofore unavailable insight into storm electrification processes, yielding data on lightning

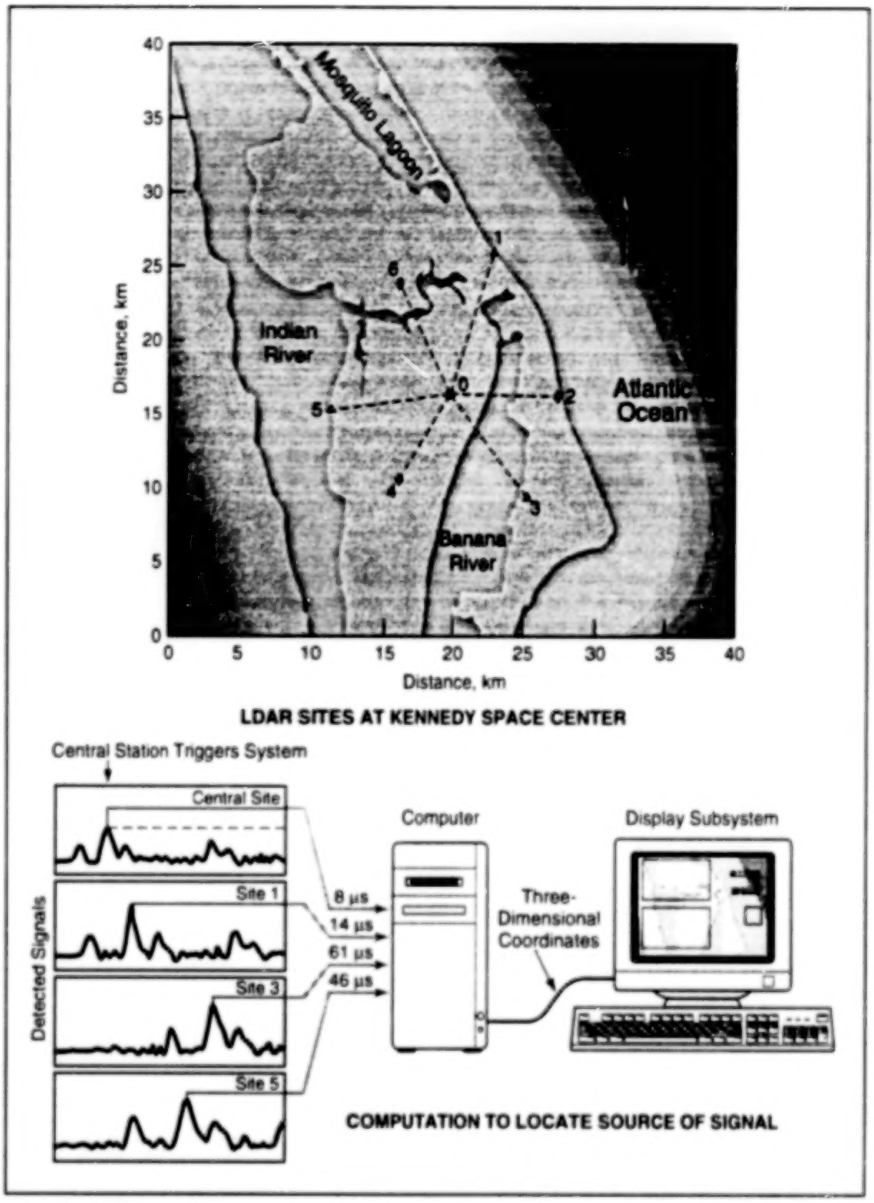

The LDAR System includes a central station display and 6 remote stations that monitor radiation at a frequency of 66 MHz to detect lightning flashes. The location of a flash is computed from differences among the times of arrival of signals from that flash at the various stations.

core heights and their meteorological dynamics. This ability could potentially lead to such benefits as improved microburst warnings for airports and passengers, in addition to obvious research implications. On a second-by-second basis, from the displayed structure of lightning sources, a user can determine whether a lightning core is vertical or geographically dispersed. The lightning core is easy to discern, as detected lightning sources extend from the ground to a height of 16 km. The stratified regions of the lightning activity are also evident and provide valuable information about the maturity of a storm.

This work was done by Thomas O. Britt, Carl L. Lennon, and Launa M. Maier of **Kennedy Space Center**. *No further documentation is available.*

Inquiries concerning rights for the commercial use of this invention should be addressed to the Patent Counsel, Kennedy Space Center [see page 1].

This technology is being developed through NASA's Dual Use Technology Development Program, where NASA and their partner Global Atmospherics, Inc., are jointly funding the developmental effort.

Inquiries concerning the commercial use of this technology should be addressed to
Ken Cummins, VP Engineering
Global Atmospherics, Inc.
2705 East Medina Rd.
Tucson, AZ 85706-7155
Tel.: 1-520-741-2838

Refer to KSC-11785, volume and number of this NASA Tech Briefs *issue, and the page number.*

General-Purpose Optically Powered Sensor and Control System

Both power and data are transmitted via optical fibers.

NASA's Jet Propulsion Laboratory, Pasadena, California

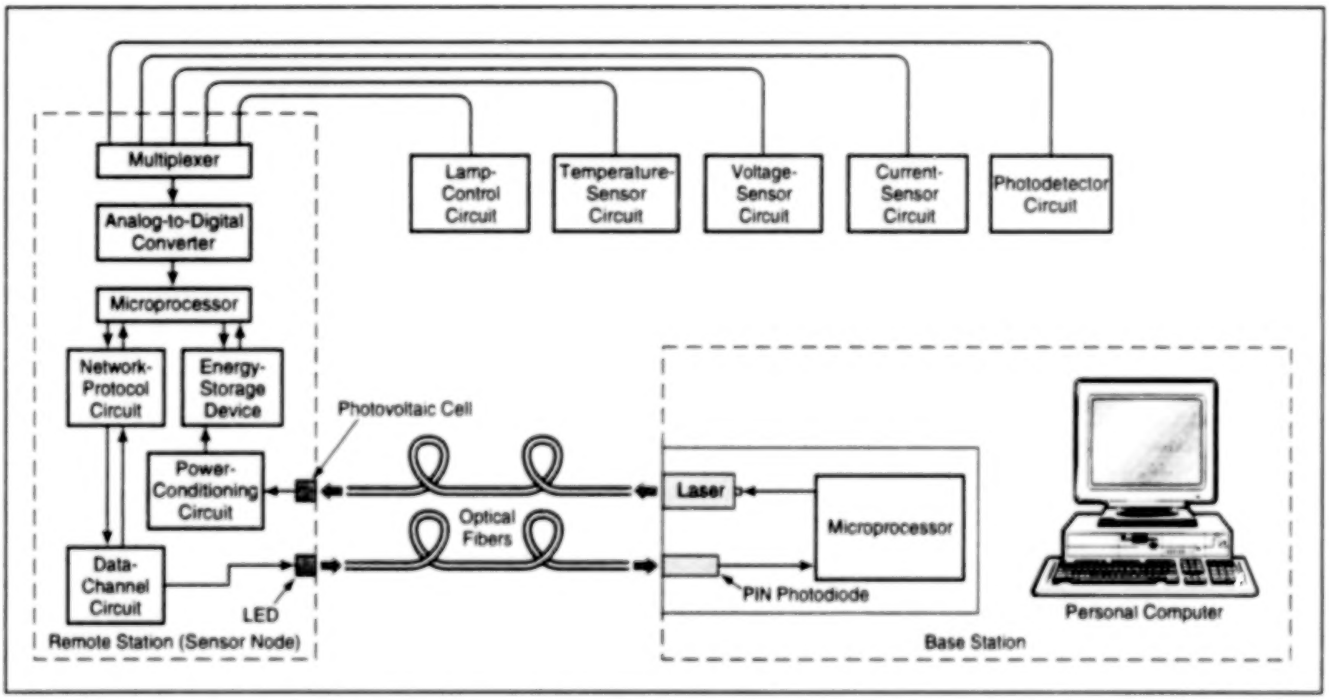

The **Prototype Optically Powered Sensor and Control System** has been used to measure a voltage, a current, and a temperature; to turn a lamp on and off; and to verify that the light is on or off.

The figure schematically illustrates a prototype general-purpose, microprocessor-based sensor and control system in which power, data, and control signals are transmitted via optical fibers. This system serves as an experimental model for the further development of networks of remote sensors connected to monitoring and controlling base stations via optical fibers.

In one important class of potential applications, networks of the type envisioned would be embedded in structures to monitor strains and vibrations. Another important class of potential applications would take advantage of the electrical isolation afforded by optical fibers; networks of sensors could be deployed to monitor voltages and currents and/or to command the operation of switches at critical locations along high-voltage power lines. Some aspects of systems that might eventually be developed were discussed in "Fiber-Optic Distribution of Pulsed Power to Multiple Sensors" (NPO-19420), *NASA Tech Briefs*, Vol. 20, No. 5 (May, 1996), page 18a and "Data Protocol for Optically Powered Sensors" (NPO-19421), *NASA Tech Briefs*, Vol. 21, No. 6 (June, 1997), page 6a.

In the present system, power for the remote station (sensor node) is supplied by a small laser of the type used in compact-disc players. The laser light is transmitted via an optical fiber to the remote station, where a photovoltaic cell converts the light to electric power. By modulating the laser light, the base station can transmit commands to the remote station; this amounts to an optical analogue of the established power-line-carrier technique, in which an electric power line is used to carry small ancillary control or data signals superimposed on the main power signal.

At the remote station, the outputs of sensors are multiplexed, digitized, and preprocessed, and the resulting data are converted to pulses of current supplied to a light-emitting diode (LED). The resulting pulses of light from the LED are transmitted

along a second optical fiber to the base station, where a PIN (positive/intrinsic/negative) photodiode converts the light pulses to electrical data pulses. The returned sensor data are sent to a personal computer for further processing and display.

The operations of the base and remote stations are controlled by microprocessors. The microprocessor in the remote station is of a low-power type and is programmed with software that puts the remote-station circuitry into a low-power "sleep mode" most of the time to conserve energy. When needed, this circuitry can be "awakened" by transmitting a command via the power-supply optical fiber.

This work was done by Harold Kirkham, Larry A. Bergman, Shannon P. Jackson, Alan R. Johnston, and Duncan Liu of Caltech for **NASA's Jet Propulsion Laboratory**. *Further information is contained in a TSP [see page 1].*
NPO-19604

Transmitting Power to Sensor Circuitry via Modulated Light

The power-conversion circuit in the sensor node can be made simpler and more efficient.

NASA's Jet Propulsion Laboratory, Pasadena, California

Modulated (as opposed to steady) light can be used in the optical transmission of power to remotely located sensor circuitry in a system like that described in the preceding article, "General-Purpose Optically Powered Sensor and Control System" (NPO-19604). This is analogous to the use of alternating (as opposed to direct) current on electrical power lines, and the benefit is similar; namely, that the voltage can be stepped up to a desired level by use of a transformer.

The figure illustrates two alternative techniques as well as the present technique for fiber-optic transmission of power from a base station to a remote station (sensor node) and conversion of optical to electrical power at the remote station. In the first technique, steady light is sent to an array of photodiodes, which are connected in series to build up the voltage to the required level. The disadvantage of this technique is that an array of photodiodes can be expensive, and there can be significant losses in the coupling of light from the optical fiber to the array, depending on the shape of the array.

In the second technique, steady light is sent to a single photodiode, and the output steady voltage of the photodiode is increased to the required higher level by a chopper, a step-up transformer, and a rectifier. The disadvantage of this technique is that the chopper consumes a substantial part of the power, thereby reducing the overall power-conversion efficiency of the remote station.

In the present technique, the optical power is modulated at the source in the base station, where efficiency is somewhat less of a consideration because power is more abundant there. Preferably, the light is either modulated with a sine wave or is chopped into square pulses ("on" during the first half cycle, "off" during the second half cycle). The modulated light illuminates a single photodiode, the output of which is now modulated. The modulated output of the photodiode is fed directly to a step-up transformer; because of the modulation, there is no need to process it through a chopper. Therefore, the chopper is eliminated and the power-conversion efficiency correspondingly increased. In practice, the conversion efficiency will not be high unless care is taken in the design of the step-up transformer and the rectifier circuit. Techniques to recover the magnetic energy in the transformer that are similar to those used in chopper circuits should be used.

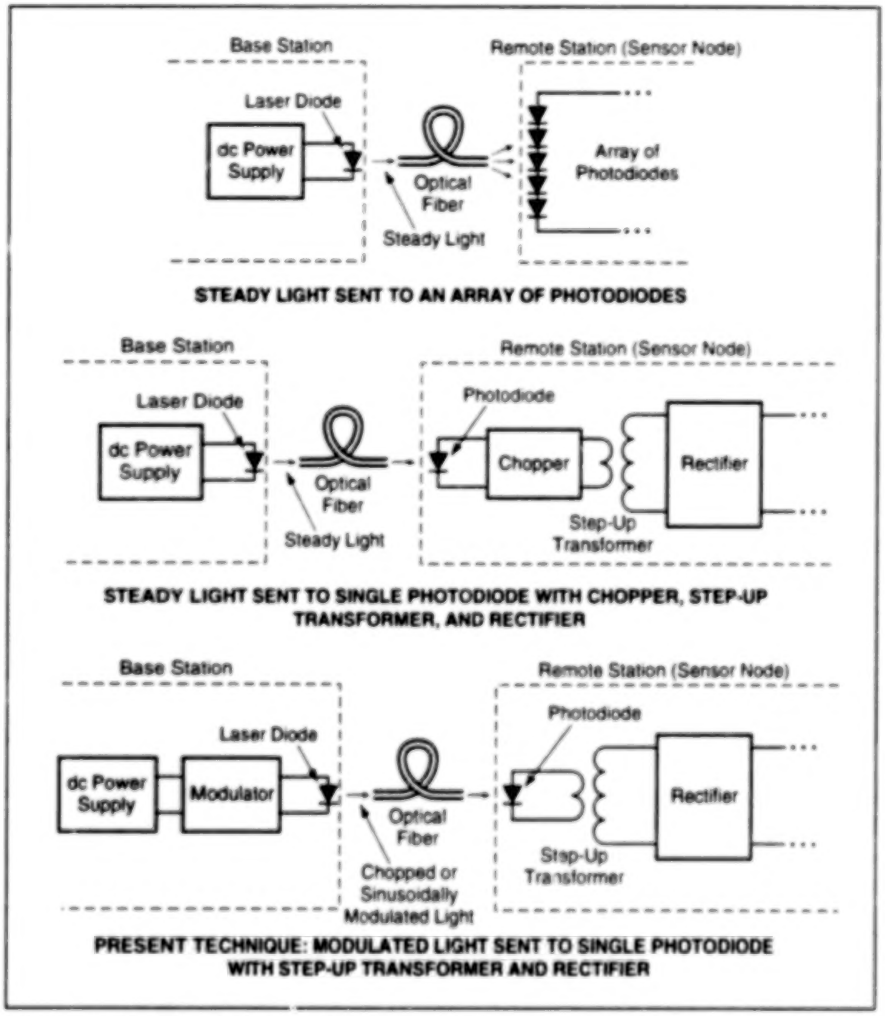

The Optical-to-Electrical Power-Conversion Circuit in the remote station can be simplified and made more efficient when modulated light is used, because there is no need for a power-hungry chopper.

This work was done by Shannon P. Jackson, Harold Kirkham, and Colonel McLyman of Caltech for **NASA's Jet Propulsion Laboratory**. *Further information is contained in a TSP [see page 1].*
NPO-19603

Transmitting Data Signals via Fiber-Optic Power Lines

Optical power carrier signals are modulated with data signals.

NASA's Jet Propulsion Laboratory, Pasadena, California

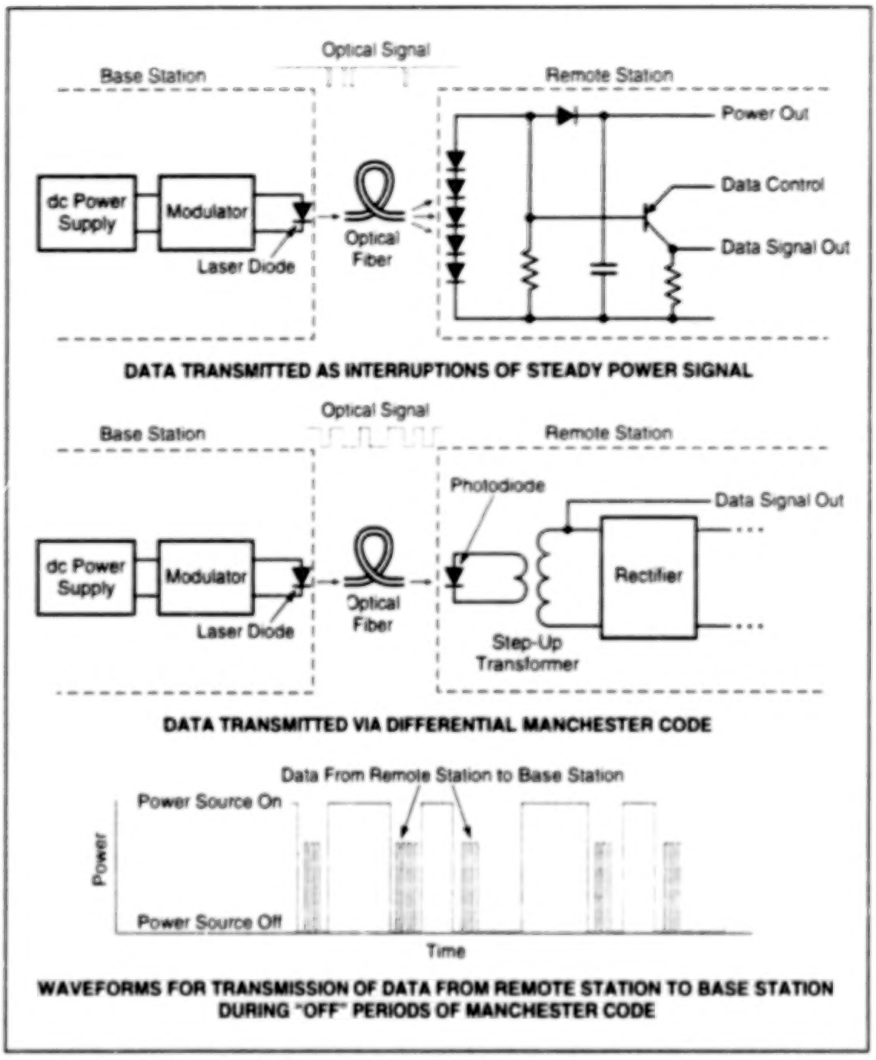

Optical Data Pulses Can Be Transmitted from the base station to the remote station as interruptions of an otherwise steady optical power-supply signal. Higher-frequency data pulses can be transmitted back to the base station during the "off" periods of the Manchester code.

Data signals can be transmitted via the same optical fibers that are used to transmit power from base stations to remote stations containing sensors and associated circuitry. [A prototype system based on fiber-optic transmission of data and power is described in "General-Purpose Optically Powered Sensor and Control System" (NPO-19604), which is the first of two articles preceding this one.] The implementation of the present data-transmission/power-transmission concept involves the choice of one of several possible modulation schemes (see figure); the choice of a scheme for a specific system depends, in part, on whether the power-supply optical signal is steady or is modulated as described in the immediately preceding article, "Transmitting Power to Sensor Circuitry via Modulated Light" (NPO-19603).

In the case of a nominally steady power-supply optical signal, the data modulation can consist of brief interruptions of this signal; the modulation can be picked off by a simple amplifier circuit added to the power-conversion circuit in the remote station. In an experiment, data were transmitted at rates as high as 9.6 kb/s. The power-conversion circuit can be designed with sufficient reserve capacity and with a capacitor or other energy-storage device to supply power to the other circuits in the remote station during the interruptions.

If the power-supply optical signal is nominally a steady pulse train in which the light is on half the time and off half the time, then the pulse train can be modified for transmission of data by the differential Manchester code. In the absence of data, the pulse train continues undisturbed; when data are present, some of the "on" pulses are changed to "off" pulses, and an equal number of "off" pulses are changed to "on" pulses. Because the total numbers of "on" and "off" pulses remain the same, the time-averaged transmitted power does not change.

In principle, it should also be possible to transmit data from the remote station back to the base station along the power-supply optical fiber. A microprocessor-controlled data-transmission optoelectronic circuit in the remote station would be synchronized with the Manchester-code pulses; during the "off" periods of the Manchester code, this circuit would transmit trains of relatively high-frequency data pulses.

This work was done by Shannon P. Jackson and Harold Kirkham of Caltech for **NASA's Jet Propulsion Laboratory**. *Further information is contained in a TSP [see page 1].*

NPO-19605

Impedance-Based Cable Tester

Short and open circuits can be located relatively easily.

John F. Kennedy Space Center, Florida

The figure illustrates the major functional blocks of an impedance-based cable-testing apparatus that can locate an open or short circuit in a cable. There is no need to disconnect the cable from all other equipment in preparation for a test — an advantage in a system in which cable connections are located in places that are not readily accessible.

The cable tester is based on the concept of a cable as a transmission line, and on exploiting the impedance-transformation property of a transmission line that is a quarter wavelength long at some frequency: If one end of a quarter-wavelength-long transmission line is short-circuited, then the transmission line presents infinite impedance in the ideal case (or very high impedance in practice) to any equipment connected to the other end. If one end is open-circuited, then the transmission line presents zero impedance in the ideal case (or very low impedance in practice) to any equipment connected to the other end.

In the cable tester, a numerically controlled oscillator generates a sinusoidal signal at a frequency chosen by a microprocessor. (In the prototype tester, the frequency can lie between 500 kHz and 40 MHz.) The signal is amplified, and the resulting output signal is fed through a reference resistor (R) into the cable at an accessible point. The voltage V at the output terminal of the amplifier and the voltage V_0 at the point of connection to the cable are measured. Then the impedance (Z) presented by the cable at the point of injection of the signal is given by

$$Z = RV_0/(V - V_0).$$

To obtain the exact value of Z, it would be necessary to measure both the magnitudes and the phases of V and V_0. In practice, it suffices to measure the magnitudes only, because under a short- or open-circuit condition, V_0 must be close to zero or V, respectively.

The tester operates as follows: The microprocessor commands the oscillator to start at the lower end of its frequency range and sweep through increasing frequency until the impedance given by the above equation either falls to near zero or else rises to ≥10 times the nominal impedance of the cable. A near-zero-impedance indication signifies an open circuit in the cable; a high-impedance indication signifies a short circuit in the cable.

The distance d along the cable from the point of injection of the signal to the short or open circuit is then simply a quarter wavelength at the frequency (f) at which the sweep was stopped:

$$d = cv/(4f),$$

where c is the speed of light and v is the velocity factor of the cable (typical velocity factors range between 0.6 and 0.9). With the frequencies used in the prototype tester, it has been possible to locate short or open circuits at distances from about 1 to 150 m from the point of injection.

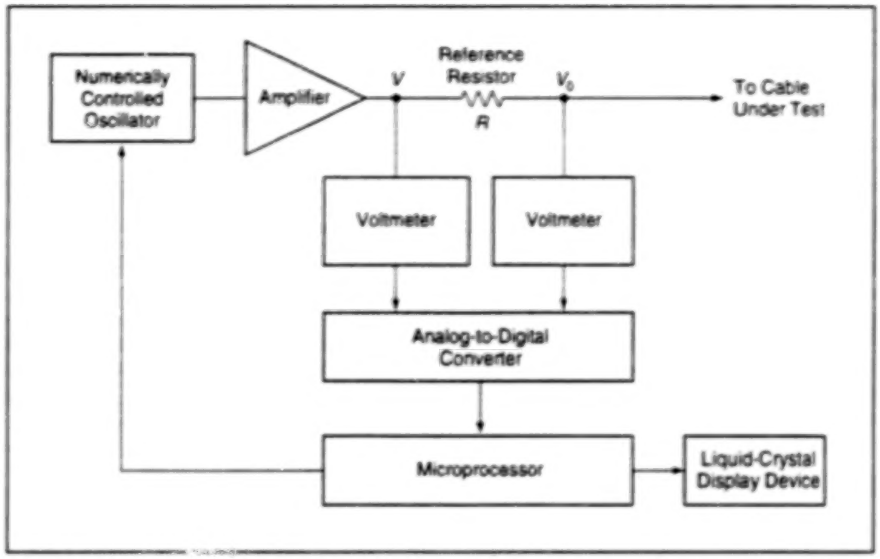

The **Impedance-Based Cable Tester** detects and locates an open or short circuit in a cable by a method that exploits the impedance-transformation property of a quarter-wavelength transmission line. The tester can be constructed as a battery-powered, hand-held, portable instrument.

The electronic circuitry of the tester can readily be integrated into a hand-held, portable instrument that runs on batteries. Such an instrument would have great commercial potential; for example, it could reduce the time spent in diagnosing cables and electronic equipment connected to cables in airplanes.

This work was done by Pedro J. Medelius and Howard J. Simpson of Dynacs Engineering Co., Inc., for **Kennedy Space Center**. *Further information is contained in a TSP [see page 1].*

This invention is owned by NASA, and a patent application has been filed. Inquiries concerning nonexclusive or exclusive license for its commercial development should be addressed to the Patent Counsel, Kennedy Space Center; (407) 867-6225. Refer to KSC-11866.

Low-Frequency Signal-Pickup Cable Tester

Careful design enables use of a test signal frequency much lower than usual.

John F. Kennedy Space Center, Florida

A cable-testing apparatus has been designed for use in detecting a short or open circuit in a cable, subject to a special frequency requirement as explained in the next paragraph. This cable tester is based on the injection of a signal at one end of the cable and the use of a pickup coil placed adjacent to the cable to detect the signal. The pickup coil is moved along the outside of the cable until the signal is lost; the loss of signal indicates the location of a short or open circuit.

Commercial cable testers based on this principle inject signals with frequencies of several hundred kilohertz. In the specific application for which the present cable tester was developed, the cable is shielded, and there is a special requirement to use a frequency of 10 Hz; this requirement is dictated by the frequency responses of signal processors connected to the cable. The use of this frequency in a shielded cable poses two challenges to effective signal-pickup cable testing: (1) at such a low frequency, the shield becomes almost 100 percent effective, so that there is very little signal power that leaks through to the outside; and (2) for a given magnetic-field signal amplitude, the output of a pickup coil is directly proportional to the signal frequency.

These challenges are overcome by use of a narrow-band-pass filter followed by a high-gain amplifier. The filter is needed to minimize the noise that enters the amplifier along with the weak signal that coil

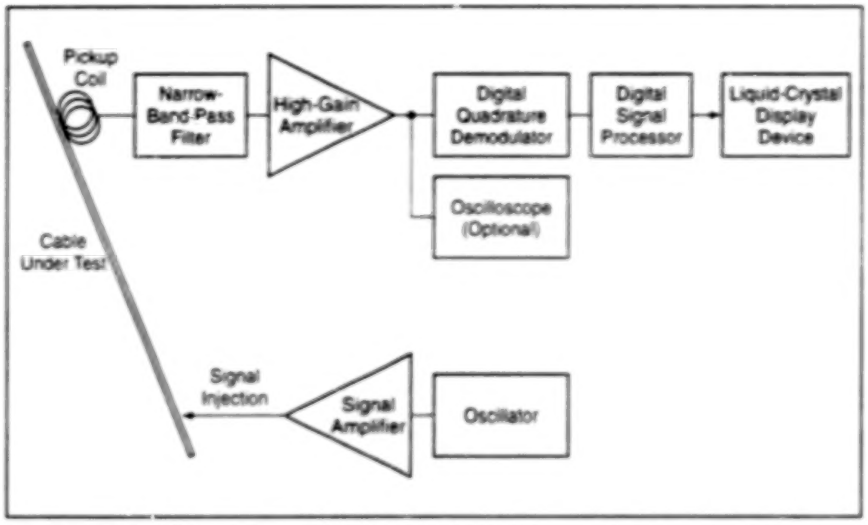

The Narrow-Band-Pass Filter and High-Gain Amplifier are needed because of the extreme weakness of the signal picked up by the coil.

picks up from the cable; the amount of this noise is proportional to the bandwidth of the filter, and thus one should make the bandwidth as narrow as practicable. The filter is of 16th order and exhibits a bandwidth of 0.05 Hz with a center frequency of 10 Hz. Both the signal frequency and the center frequency are crystal-controlled to prevent drifts that would degrade signal-pickup performance.

The output of the amplifier is detected, using a digital quadrature demodulator. Optionally, the output of the amplifier can also be displayed on an oscilloscope. Like the tester described in the preceding article, this one has commercial potential, especially for use in the aircraft industry.

This work was done by Pedro J. Medelius of Dynacs Co., Inc., for **Kennedy Space Center.** *Further information is contained in a TSP [see page 1].*

This invention is owned by NASA, and a patent application has been filed. Inquiries concerning nonexclusive or exclusive license for its commercial development should be addressed to the Patent Counsel, Kennedy Space Center; (407) 867-6225. Refer to KSC-11865.

In-Process Monitoring and Analysis of Thermal-Spray Processes Using Machine Vision

Optical probe captures images of fast-moving particles in a plasma-spray chamber.

Marshall Space Flight Center, Alabama

The LaserStrobe Optical Probe is an advanced laser-augmented video-imaging system that observes and measures particle behavior in the harsh environment of a plasma-spray chamber. The need for a reliable diagnostic and feedback control system during thermal-spray processing spurred the development of this sophisticated system.

LaserStrobe is intended to enable manufacturers of aerospace engine components to reduce production costs, while meeting the strict standards of quality for parts that are commonly coated using the plasma-spray process.

The conditions inside the low-pressure chamber during plasma-spray processes include an extremely bright plasma flame, strong electromagnetic fields, high temperature, and contamination from powder overspray circulating throughout the chamber during operation. LaserStrobe was designed to endure this harsh environment and enable scientists and engineers to measure parameters such as particle velocity and particle distribution during the spraying process.

This water-cooled optical probe has a pulsed laser illumination system and a special-purpose camera head that provide images of extremely bright industrial processes — such as electric arc welding and plasma spray. The optical probe components are attached to a 14-in. (29-cm) diameter flange. The flange is then mounted on the main access door of the plasma-spray chamber.

Figure 1. The LaserStrobe Optical Probe assembly is mounted to the main access door of the plasma-spray chamber to protect the components of the system during operation.

Figure 2. The Optical Probe camera provides clear video of "twin imagery" of the particle dynamics inside the plasma-spray chamber.

The LaserStrobe Optical Probe system was installed and tested in the Low-Pressure Plasma Spray chamber at Marshall Space Flight Center in Huntsville, Alabama. Two fan-shaped laser beams are superimposed in the focal plane of the camera head, providing two spot images of each traveling particle in the video frame. With a few microseconds of delay between the first and second laser pulse, "twin images" are produced as the particles move across the camera field of view. During these tests, the optical probe system provided clear imagery of plasma- spray plume particles inside the chamber.

This work was done by Jon D. Bolstad, John C. Lagerquist, and Craig L. Shull of Control Vision, Inc., for **Marshall Space Flight Center.** *Further information is contained in a TSP [see page 1].*

Inquiries concerning rights for the commercial use of this invention should be addressed to the Patent Counsel, Marshall Space Flight Center [see page 1]. Refer to MFS-26424.

Physical Sciences

Hardware, Techniques, and Processes

Books and Reports

BLANK PAGE

Autostereoscopic Displays for Scientific Visualization

Flat-screen three-dimensional displays have been developed to enhance visualization of scientific and other images.

Dimension Technologies Inc., Rochester, New York

Many types of scientific images and data are complex and are easier to interpret when observed in three dimensions. This is especially true for information presented visually in the form of multiparameter graphs and tables, as well as for images of physical events, such as turbulent flows. Furthermore, the appearance of depth in stereoscopic displays adds greatly to the understanding and analysis of scientific imagery, especially of physical events. This is, of course, true for other images as well — wherever rendition of depth is important — for example, in mechanical engineering, architecture, medicine, and other fields of endeavor.

Dimension Technologies Inc. (DTI) has developed and patented a unique method for generating three-dimensional images by use of stereo pairs. Much of this work has been done under contracts from NASA and other federal agencies. The project described here was successfully carried out in close cooperation with NASA Ames Research Center under a Small Business Innovation Research (SBIR) contract. The results of this work have been commercialized, and an innovative autostereoscopic display, the Virtual Window™, shown in Figure 1, was introduced.

Unlike other stereoscopic displays, this unit generates vivid, full-color three-dimensional images that can be viewed without the need to wear special eyeglasses. This feature makes the use of the autostereoscopic displays very convenient and is particularly important in commercial applications.

The principle of autostereoscopic image presentation is frequently used in three-dimensional postcards and large advertising displays that are intended to enable the observer to perceive depth by looking at a two-dimensional picture. A stereo pair (i.e., a pair of images corresponding, respectively, to the views through the left and right eyes) are interlaced in alternate columns in a two-dimensional image. A special optical device, called the "lenticular lens," is placed in front of the interlaced image or, in the case of a postcard, bonded directly to the front surface. The lenticular lens is an array of very narrow vertical cylindrical lenslets spaced to correspond to the columns of the interlaced stereo pair. In this manner, the appropriate images of the stereo pair are directed to the proper eyes thus generating a three-dimensional image.

Figure 1. This Virtual Window™ Flat-Panel Display features a 12.1-in. (30.1-cm) viewable area, 1024 × 768 resolution, and can work with PC and Mac platforms.

As illustrated in Figures 2(a) and (b), DTI has applied the same principle to its autostereoscopic displays, which contain liquid-crystal displays (LCDs) that are viewed by observers. To generate three-dimensional images, the LCD presents left and right halves of a stereo pair on alternate columns of pixels at a rate of 60 frames per second. The left image appears on the odd columns and the right image appears on the even columns. If the LCD in use has 1,024 columns and 768 rows of pixels, each complete stereoscopic image consists of 512 columns and 768 rows.

Both halves of a stereo pair are displayed simultaneously and directed to the corresponding eyes. This is accomplished with a special illumination plate located behind the LCD and employing a lenticular lens of the type mentioned above. Using light from compact, intense light sources, the illumination plate optically generates a lattice of very thin, very bright, uniformly spaced vertical light lines. The lines are precisely spaced with respect to pixel columns of the LCD, and, because of the parallax inherent in binocular vision, the left eye sees all of these lines through the odd columns of the LCD, while the right eye sees them through the even columns, thus enabling the observer to perceive the image in three dimensions. This arrangement, exclusive to DTI, is called "parallax illumination."

There is a fixed relation between (1) the distance between the LCD and the illumination plate and (2) the distance between the observer's face and the LCD screen (the viewing distance) that in part determines the dimensions and

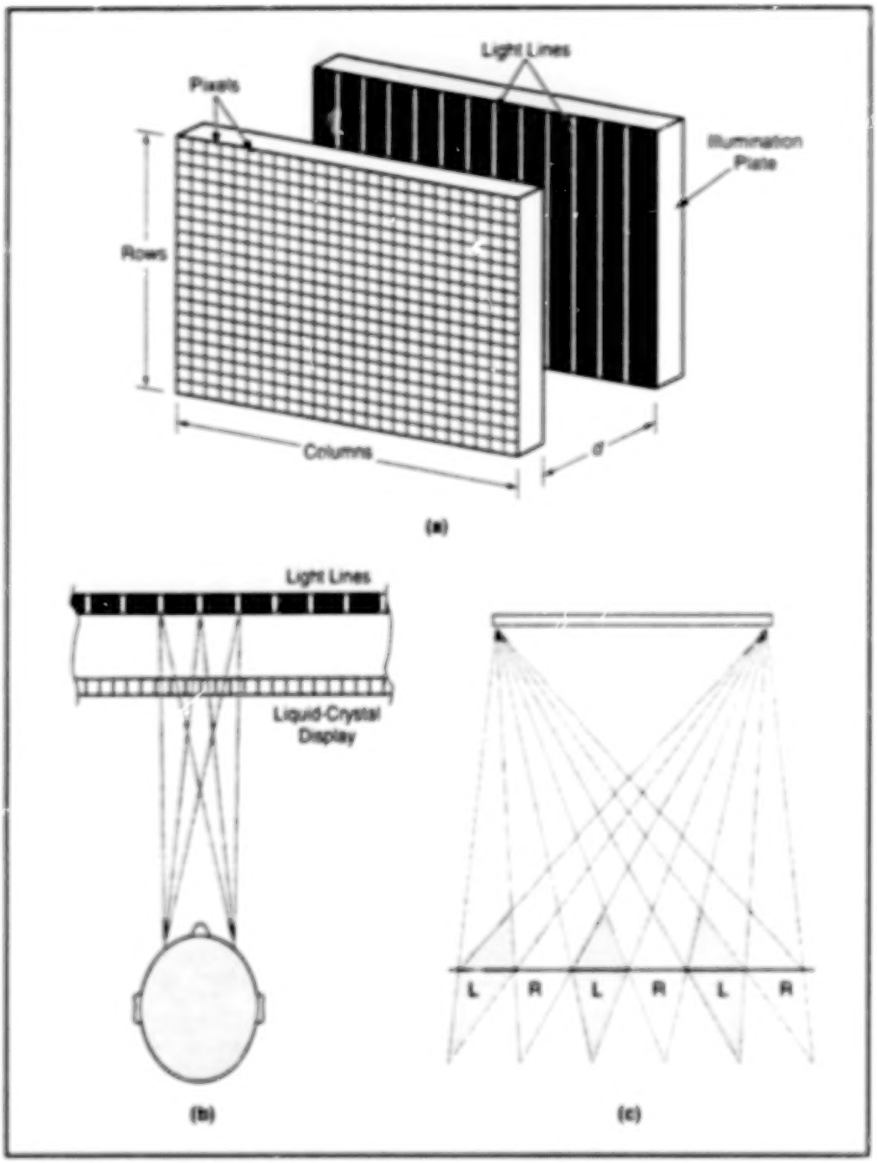

Figure 2. **Some of the Principles** behind these autostereoscopic displays involve (a) LCD and the illumination plate, (b) geometric relationship between the light line and the LCD pixel, and (c) the viewing zones in front of the display where the observer perceives three-dimensional images.

positions of the "viewing zones," which are depicted in Figure 2(c). These viewing zones are the regions in front of the display where the observer can perceive three-dimensional images.

When the halves of the stereo pair are made to correspond to the scene perspective that would naturally be seen by the respective eyes, a vivid illusion of three-dimensionality is created. The objects seem to come out of the screen, giving the impression of an open window through which objects can protrude or retreat to the background — hence, the name Virtual Window™. In addition, the parallax illumination system is designed such that it can generate in the same display, at a flick of a switch, both the stereoscopic and non-stereoscopic images — the latter at double the resolution.

The displays are compatible with computer workstations, including PC and Power Mac platforms, and accept real-time inputs through multiplexers in National Television Systems Committee (NTSC) and PAL formats from pairs of video cameras.

It is possible to produce displays that enable several people to view in stereo at the same time. The displays are light in weight and are available at moderate cost.

Efforts continue to further enhance the Virtual Window™ displays to obtain greater resolution, and to provide for generation of hologramlike imagery, in which objects can be observed from different perspectives, and, most importantly, in developing applications. For scientific applications, some areas of interest include the display of multidimensional graphs and tables, molecular structures, turbulent flows, biological and artificial structures, and images obtained by use of stereo microscopes. Other applications include remote control of vehicles and robots, inspection of luggage and parcels, quality assurance in the production of semiconductor devices and other miniature structures, aircraft and spacecraft cockpit displays, interpretation of aerial photography, medical imaging including endoscopy, and, last but not least, such consumer products as video games and three-dimensional television.

This work was done under the direction of Jesse Eichenlaub, Chief Scientist, by **Dimension Technologies Inc.**, *315 Mt. Read Blvd, Rochester, NY 14611, (716) 436-3530, under an SBIR contract monitored by* **NASA's Ames Research Center**. *Reported by Alexander E. Martens, Executive Director, Upstate CTC, Rochester, NY 14625.*

Multimode Optical Fiber as Imaging Probe

Phase conjugation in a hologram would provide compensatory prescrambling.

NASA's Jet Propulsion Laboratory, Pasadena, California

A proposed electro-optical image-processing system would enable remote viewing of an object through a multimode optical fiber, as though the fiber were a conventional image-transmitting optic like a lens or prism. Ordinarily, it would be impractical to use a multimode optical fiber as an imaging probe or imaging optic because image information would become distorted (scrambled) during propagation along the fiber. The proposed system would provide compensation for this scrambling. Fiber-optic imaging probes of this type could be made very thin and could be particularly useful as minimally invasive probes in medical diagnosis.

The system (see figure) would include two multimode optical fibers, which would

be terminated side by side at one end (point A) facing the object that one seeks to view. The tips of the fibers would lie at a short distance, *s*, from the object. A source of light at point C would illuminate the object via fiber 2. An observer at point B would attempt to view the illuminated object through fiber 1. The problem is to predistort the illumination (prescramble the amplitudes and phases of the fiber-optic waveguide modes of the illuminating electromagnetic field) in such a way as to compensate for the scrambling that occurs during transmission of the image along fiber 1 from point A to point B, so that the image of the object would arrive unscrambled at point B.

The solution would involve the generation and use of a hologram in a phase-conjugating crystal at point C. First, a flat mirror would be placed facing the tips of the optical fibers, where the object would later be placed for viewing. A source of light would be placed at point A (where the observer would later be stationed). Light from this source would travel through fiber 1 to point A, where it would be reflected into fiber 2. Upon emerging from fiber 2 at point C, the light would enter the crystal. At the same time, the crystal would be illuminated with a reference (plane-wave) beam of light. Interference between the reference beam and the light emerging from fiber 2 would produce the desired hologram, which would encode the information about scrambling in both fibers 1 and 2.

Once the hologram had been generated, one could exploit the phase-conjugation principle to reverse the propagation of the optical signal and thus reverse scrambling. The crystal would be illuminated with the phase conjugate of the reference beam (in essence, a beam of the same wavelength propagating along the reverse of the path of the reference beam); this would cause reverse-propagation with unscrambling of light from point C back to point A then back to point B. If the mirror were replaced by the object to be viewed, then the reverse-propagating light would illuminate the object and the image of the object would spatially modulate the reverse-propagating beam, such that an undistorted image of the object would appear at the completion of reverse propagation and unscrambling at point B.

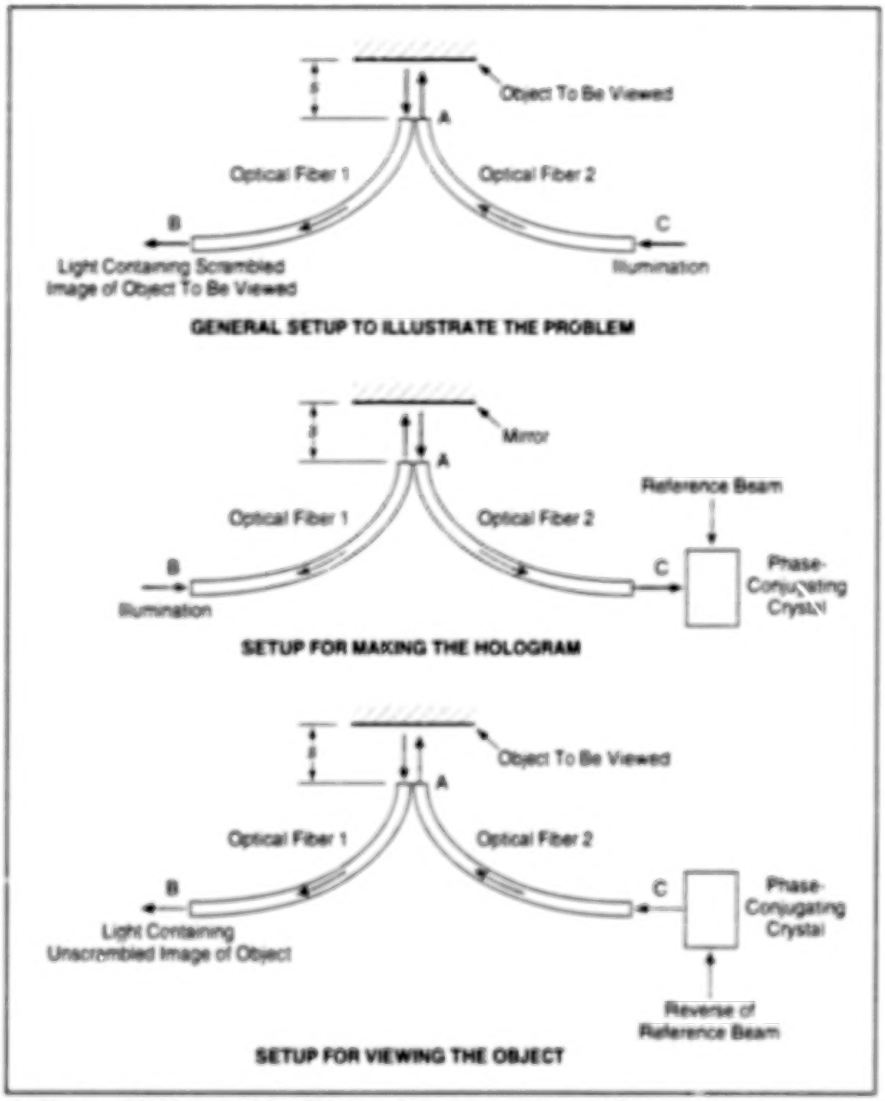

An Unscrambled Image of the Object could be generated at point B by exploiting phase conjugation at point C to reverse the scrambling that occurs during propagation along the optical fibers.

This work was done by Deborah Jackson of Caltech for **NASA's Jet Propulsion Laboratory** *Further information is contained in a TSP [see page 1].*
NPO-19671

Sonochemical Treatment To Remove Hydrazines From Water

There would be no need to supply a neutralizing chemical.

Lyndon B. Johnson Space Center, Houston, Texas

A sonochemical treatment has been proposed for removing hydrazine contaminants from water. The basis of the proposal is a conjecture that the sonochemical effect in water containing hydrazines would cause the hydrazines and some of the water to decompose, forming relatively innocuous products like nitrogen, ammonia, and derivatives of ammonia. On a large scale, this treatment could be incorporated into processes for remediation of industrial wastewater streams. On a smaller scale, this treatment could be effected by portable equipment that could be brought to locations where water contaminated by hydrazines has been spilled; examples of such locations include industrial chemical processing sites and spacecraft-launching sites, where hydrazines are used as hypergolic fuels.

A typical portable system (see figure) would include a wet/dry vacuum cleaner to collect the spilled water, a tank for temporary storage of the water, and a treatment subsystem that would continuously circulate water from the tank,

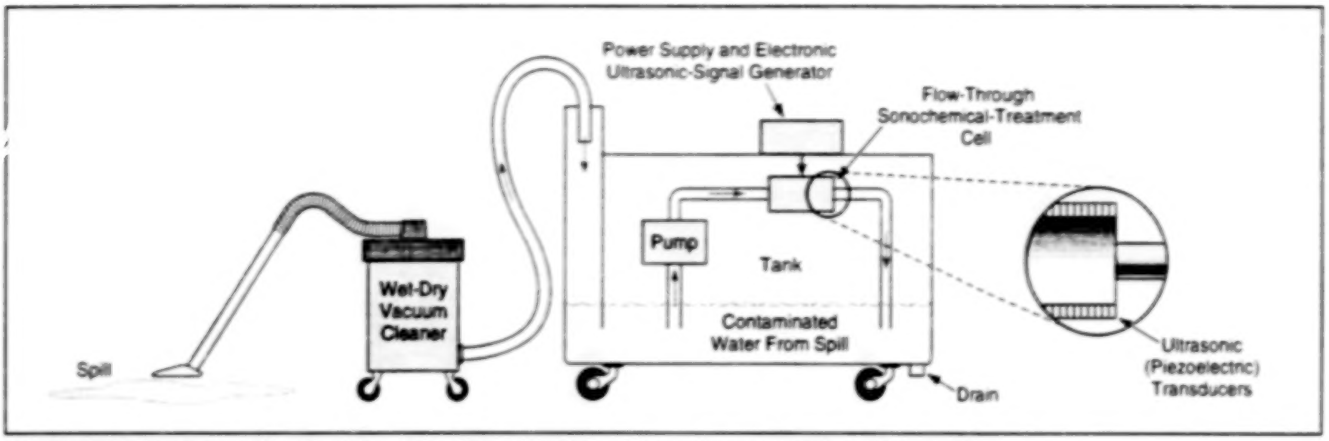

This **Portable System** would collect, then sonochemically treat spilled water contaminated with hydrazines.

through a sonochemical-treatment cell, and back to the tank. The sonochemical-treatment cell would contain piezoelectric plates that would be driven at the required ultrasonic frequency or frequencies by an external electronic source. The treatment would be continued until the concentration of hydrazines in the tank reached an acceptably low level.

This work was done by Dennis D. Davis of Allied-Signal Aerospace Co. for **Johnson Space Center**. *Further information is contained in a TSP [see page 1].*
MSC-22659

Scanning-Mode Shadowgraphy for Examining Shock Waves

One could view some shock structures that would be invisible in classical shadowgraphy.

Lewis Research Center, Cleveland, Ohio

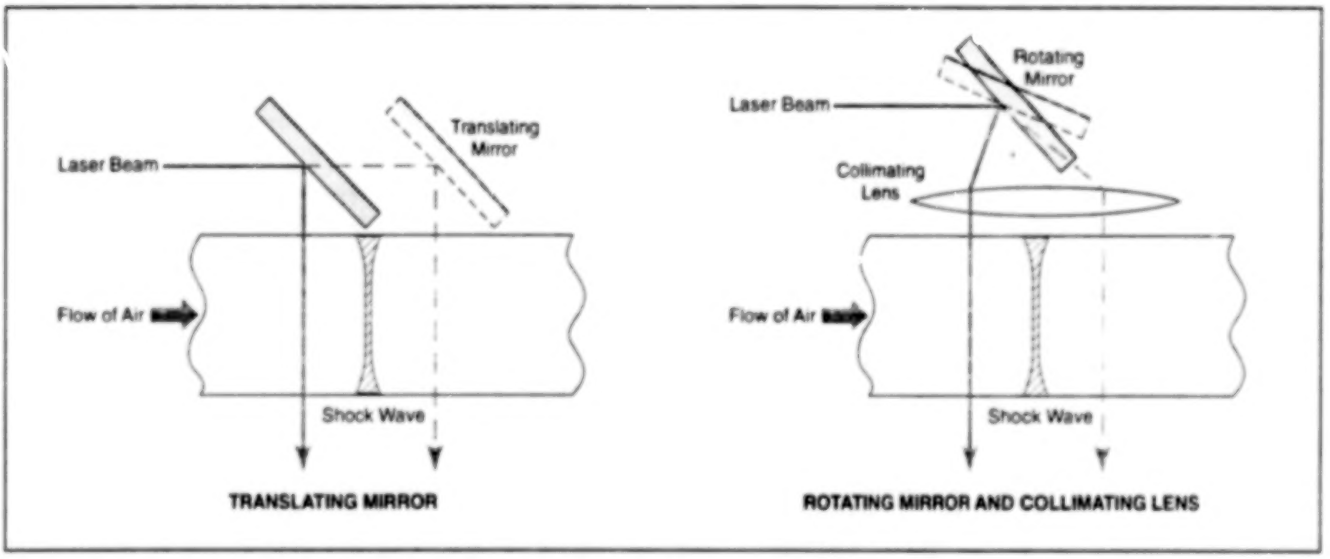

Figure 1. A **Narrow Laser Beam Could Be Scanned** along a flow region suspected of containing a shock wave.

Scanning-mode shadowgraphy has been proposed as an alternative optical technique for diagnosis of shock waves. Under suitable conditions, scanning-mode shadowgraphy could overcome the limitations of classical shadowgraphy in such a way as to make shock waves more visible and measurable.

In classical shadowgraphy, a collimated beam of light wide enough to cover the entire flow region of interest is aimed across the flow and onto a projection screen, photographic plate, array of photodetectors, or other imaging device. Any variation in the density of the flowing medium is accompanied by a variation in the refractive index and gives rise to a shadow, which alters the distribution of brightness of light striking the imaging device. Due to simplicity of this concept, shadowgraphs have been used with success in diagnosing shocks and other flow phenomena.

One limitation of classical shadowgraphy involves power density: because the beam of light is spread over a fairly wide area, either the resulting illumination is dimmer than desired, or else it is necessary to use a high-power source of light. Another limitation is that the secondary, generally weaker, phenomena caused by light diffraction and scattering on flow inhomogeneities are not visible.

In scanning-mode shadowgraphy, one would overcome the power-density limitation by collimating the light into a pencil-thin beam instead of a much wider beam. The beam could be scanned along the flow region by a translating mirror or by a rotating or acousto-optical scanning reflector placed at the focal point of a collimating lens (see Figure 1). Upon encountering a region with a strong gradient of density (e.g., a shock

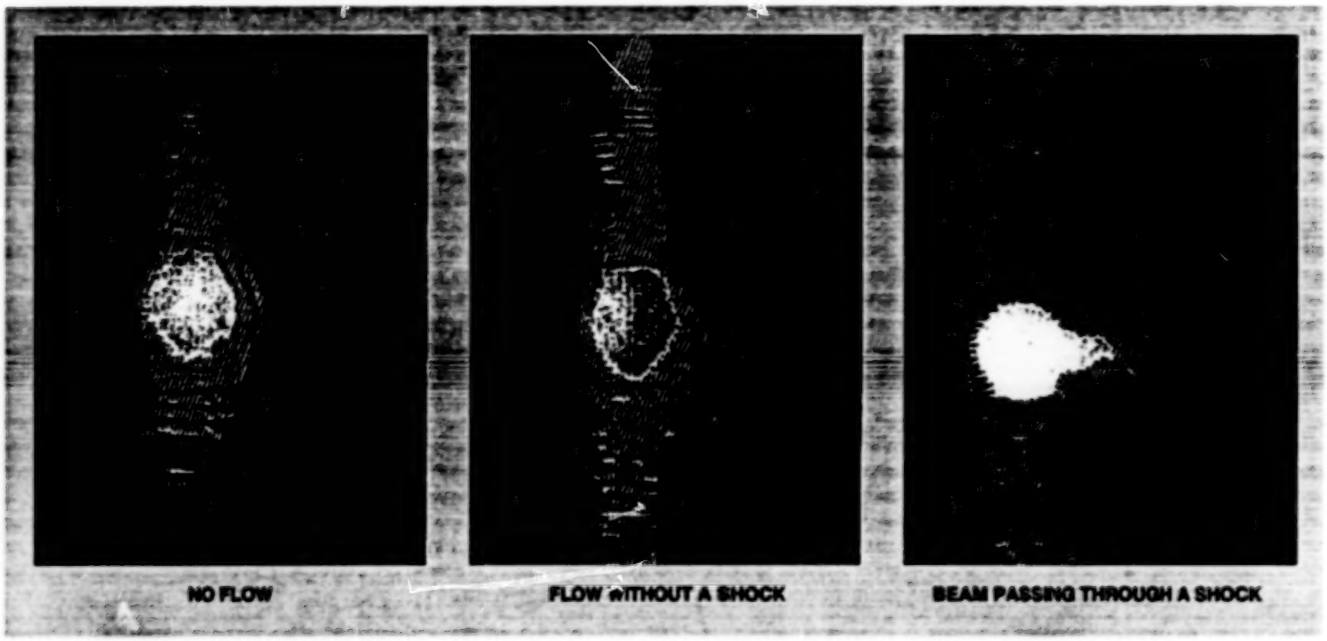

Figure 2. **A Laser-Beam Image Becomes Smeared Out** from its compact, round cross section when it crosses a shock wave.

wave), the beam would become deformed or scattered, with consequent changes in the pattern of light on the imaging device.

Experiments were conducted to compare classical and scanning-mode shadowgraphy as applied to flows of air in converging/diverging nozzles at mach numbers of the order of 2. Each nozzle was equipped with side windows. A wide, uniform beam for classical shadowgraphy was generated by a 3-mW He/Ne laser and collimating optics. A narrow beam for scanning-mode shadowgraphy was generated by a 0.5-mW He/Ne laser. Both beams were aimed through the test section of the nozzle via the windows. Figure 2 shows the results obtained in one experiment. In general, the images obtained with the scanning narrow beam revealed shocks more effectively than did the images obtained with the wider beam. This finding seems to confirm the potential of pencil-beam scanning-mode shadowgraphy for development of relatively compact, low-power apparatuses for rendering shock waves visible.

This work was done by G. Adamovsky of **Lewis Research Center** *and D. K. Johnson of the University of Akron. Further information is contained in a TSP [see page 1].*

Inquiries concerning rights for the commercial use of this invention should be addressed to NASA Lewis Research Center, Commercial Technology Office, Attn: Tech Brief Patent Status, Mail Stop 7–3, 21000 Brookpark Road, Cleveland, Ohio 44135. Refer to LEW-16427.

Measuring Flow Using Spectrally Resolved Rayleigh Scattering

Instantaneous flow can be measured simultaneously at multiple locations in a supersonic wind tunnel.

Lewis Research Center, Cleveland, Ohio

An experimental study has been conducted to demonstrate the feasibility of using spectrally resolved Rayleigh scattering to nonintrusively measure the instantaneous properties of the flow in a small supersonic wind tunnel. Unlike conventional probe flow measurements, Rayleigh scattering of a laser beam does not perturb the flow. Because the Rayleigh scattering uses the actual gas molecules that make up the flow under study, it is not necessary to seed the flow. Another important advantage of this technique is that properties of the flow can be determined simultaneously at multiple locations along the laser beam; moreover, if the laser beam is pulsed, then these flow properties can be obtained at multiple locations with a single laser pulse.

The principle of operation can be explained with the optical setup used in the feasibility study, as illustrated schematically in the figure. The main light beam for measuring the flow is generated by a pulsed, injection-seeded, frequency-doubled Nd:YAG laser, which is tuned to an absorption spectral band of iodine for the purpose of subsequent filtering, as explained below. By use of a series of lenses and mirrors, the beam is focused to a line, introduced into the wind tunnel, and directed upstream along the test section of the wind tunnel. As described thus far, this arrangement provides for Rayleigh scattering measurements from a number of regions along the illuminated downstream-to-upstream line. If the laser were sufficiently powerful, the beam-forming optics could be set to expand the laser beam to a sheet in the test section, making it possible to measure Rayleigh scattering in hundreds of regions within the test section.

The Rayleigh-scattering spectrum is directly related to the velocity distribution of the illuminated molecules; it contains information about the temperature, bulk velocity, and density of the fluid in the measurement volume. Light from the measurement volume is focused into an intensified charge-coupled-device (CCD) camera via a Fabry-Perot interferometer. The width of recorded spectrum is related to the gas temperature, the shift of the spectral peak is proportional to one component of the bulk velocity, and the total intensity is proportional to the gas density. However, the

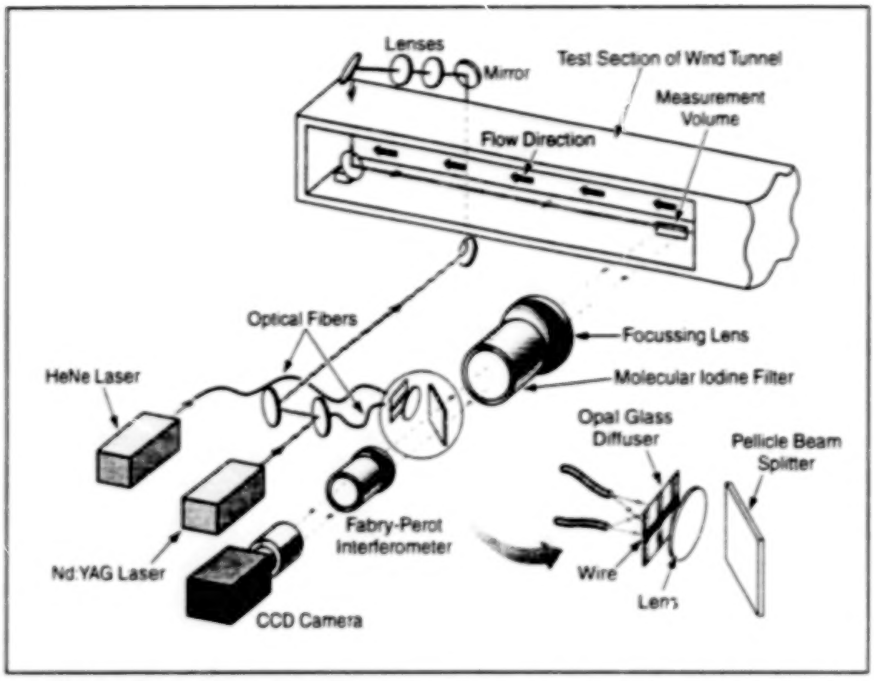

The CCD Camera Is Aimed at the Measurement Volume through a Fabry-Perot interferometer and an iodine absorption cell to obtain an image of the measurement volume in Rayleigh-scattered light. The measurement volume can be any convenient region along the laser beam in the test section of the wind tunnel.

recorded image also includes unwanted light that is not the result of Rayleigh scattering, but is caused by spurious laser scattering from windows and internal wind-tunnel surfaces. This unwanted laser light is at the laser frequency. Because the Fabry-Perot is not selective enough to eliminate this non-Rayleigh scattered light, an iodine absorption cell is placed in front of the Fabry-Perot to block light at the laser frequency.

Success in the use of the iodine absorption cell depends on knowledge of the Nd:YAG-laser frequency for each measurement. In this setup, part of the CCD is used to record simultaneously the Fabry-Perot interference-fringe patterns of (1) the unshifted light from the Nd:YAG laser, (2) light from a frequency-stabilized HeNe laser, and (3) light collected from the tunnel and filtered through the iodine cell. The frequency of the light from the Nd:YAG laser can be determined by analysis of the fringe patterns.

The apparatus performed well in the feasibility experiments. One disadvantage of this technique is the need for postprocessing of data to perform the fringe-pattern analysis to determine the frequency of the Nd:YAG laser; an on-line laser-frequency readout subsystem would be desirable in future implementations. A problem in this particular experiment was the relatively low mach number (about 2.0), which necessitated the assumption of adiabatic flow to avoid indeterminacy between velocity and temperature in the data-reduction process; however, at higher mach numbers, such indeterminacy would not occur, and therefore velocity and temperature could be determined independently of each other. The feasibility study also revealed the desirability of several improvements, including frequency stabilization of the Nd:YAG laser, vibration isolation of the Fabry-Perot interferometer, automatic (instead of time-consuming manual) alignment of the Fabry-Perot, and on-line data reduction.

This work was done by Richard G. Seasholtz and Alvin E. Buggele, of **Lewis Research Center** *and Mark F. Reeder, a National Research Council Associate. Further information is contained in a TSP [see page 1].*

Inquiries concerning rights for the commercial use of this invention should be addressed to NASA Lewis Research Center, Commercial Technology Office, Attn: Tech Brief Patent Status, Mail Stop 7-3, 21000 Brookpark Road, Cleveland, Ohio 44135. Refer to LEW-16425.

Electrochemical Monitoring of Hydrazine in Air

Concentrations as low as 10 ppb can be measured.

John F. Kennedy Space Center, Florida

An instrumentation system monitors ambient air to determine whether hydrazine vapor is present in sufficient concentration to be harmful to humans or equipment. The system can measure hydrazine concentrations as low as 10 parts per billion (ppb); this level of concentration is denoted the threshold limit value (TLV) in a revised safety standard proposed by the American Conference of Governmental Industrial Hygienists.

The system includes plumbing, electronic, and mechanical subsystems that function together to implement an electrochemical detection principle. The overall function of the system is to trap hydrazine from air in an acidic solution, adjust the pH to 10.2 for electrochemical detection, feed the solution to an electrochemical cell in a commercial process analyzer, and measure the electric current in the cell (see Figure 1).

The system includes a plastic sampling block, into which a small flow of dilute sulfuric acid is pumped. In the sampling block, the acid is dripped through an incoming flow of ambient air that could contain hydrazine vapor. The resulting mixture of air bubbles and acid is drawn from the sampling block into a sampling tube, wherein the prolonged air/acid contact results in scrubbing of hydrazine vapor from the air into the acid solution. The mixture is then drawn into a liquid/gas separator, from which the air is vented and the solution is sent for further processing.

A flow of dilute NaOH is mixed into the solution to raise the pH to ≥10.2, as required for the chosen electrochemical detection process. In this process, hydrazine is oxidized on the surface of a platinum anode in the reaction

$$N_2H_4 + 4OH^- \rightarrow 4H_2O + N_2 + 4e^-,$$

while water is reduced to hydrogen at a stainless-steel cathode in the reaction

$$4H_2O + 4e^- \rightarrow 2H_2 + 4OH^-.$$

The electrochemical cell is operated in an amperometric mode; this means that the cell current is measured while the potential applied to the working electrode (the anode in this case) is held con-

stant with respect to a reference electrode. The cell current is directly proportional to the concentration of hydrazine (see Figure 2); the constant of proportionality is established initially and verified from time to time by use of a commercial toxic-vapor-generator and flow-control equipment that generates a calibration flow of air containing a known concentration of hydrazine at known temperature and humidity.

The basic operational concentration range of the system, denoted the "TLV range," is 0 to 1,000 ppb. The system can also be operated in a range of 0 to 10 parts per million (ppm), denoted the "leak range," in which the sensitivity of detection is reduced by introducing stream of pure water to dilute the acid/hydrazine sample solution stream. Laboratory and field prototypes of the system have exhibited response times of 10 to 12 minutes in the TLV range and <2 minutes in the leak range.

The system includes reservoirs of concentrated H_2SO_4 and NaOH solutions and of deionized water. By use of automatic level-sensing and flow-control equipment, ingredients from these reservoirs are mixed as needed to obtain the dilute acidic and basic solutions for sampling and electrochemical detection. The reservoirs are sized to provide for continuous, unattended operation of the system for 3 months. To minimize the generation of waste, all effluent liquid streams generated by the system are cleaned of acidic, basic, and hydrazine residues by use of ion-exchange cartridges, then reused in the system.

This work was done by Dale Lueck of **Kennedy Space Center** *and Barry J. Meneghelli, Clyde Parrish, and Ron Barile of Dynacs Engineering Co., Inc. Further information is contained in a TSP [see page 1].*
KSC-11920

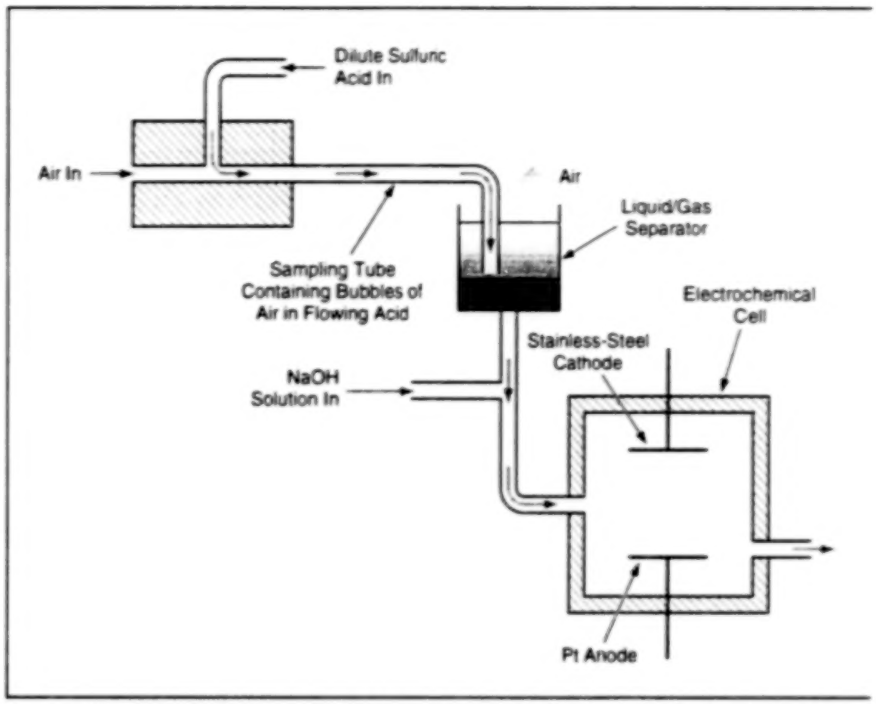

Figure 1. This **Simplified Schematic Diagram** shows the main flows used to dissolve hydrazine from air and electrochemically detect hydrazine in solution.

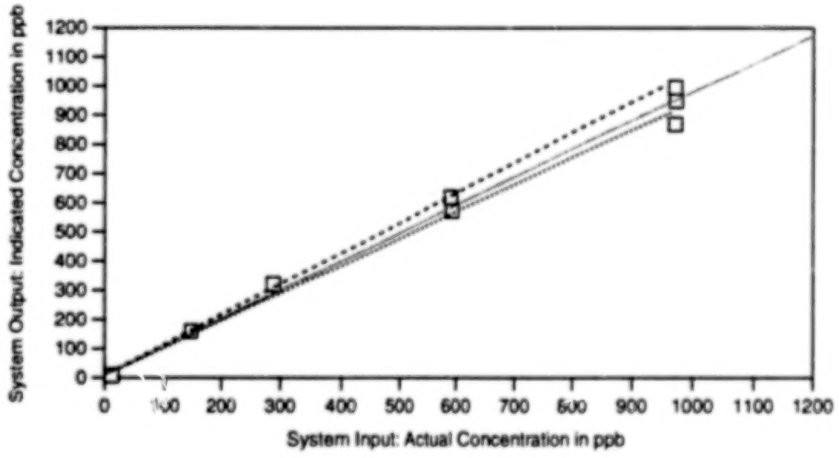

Figure 2. This **Calibration Plot** for the TLV range was obtained from measurements at known concentrations of hydrazine vapor in air. The solid line represents a best first-order fit to the experimental data. The dashed lines represent ±5-percent error around the ideal linear response.

Thermal-Desorption X-Ray Photoelectron Spectroscopy

Two techniques are combined to enhance characterization of contaminants on surfaces.

NASA's Jet Propulsion Laboratory, Pasadena, California

Thermal-desorption x-ray photoelectron spectroscopy (TDXPS) is a technique in which the thermal aspect of thermogravimetric analysis (TGA) is combined with non-angle-resolved x-ray photoelectron spectroscopy (XPS). TDXPS was developed to enhance the physical and chemical characterization of contaminants on surfaces. A combination of TDXPS and conventional XPS [including angle-resolved XPS (ARXPS)] should prove useful in industries in which surface contamination can adversely affect the results of plating, coating, and bonding processes.

XPS and TGA have different strengths and weaknesses: XPS provides both qualitative and quantitative information about chemical species (including physisorbed and chemisorbed contaminants) on solid specimens, to depths that range between 10 and 100 Å below specimen surfaces. TGA provides information on the degrees of bonding and chemical activity of those chemical species that can be desorbed from the surfaces and/or the depths of speci-

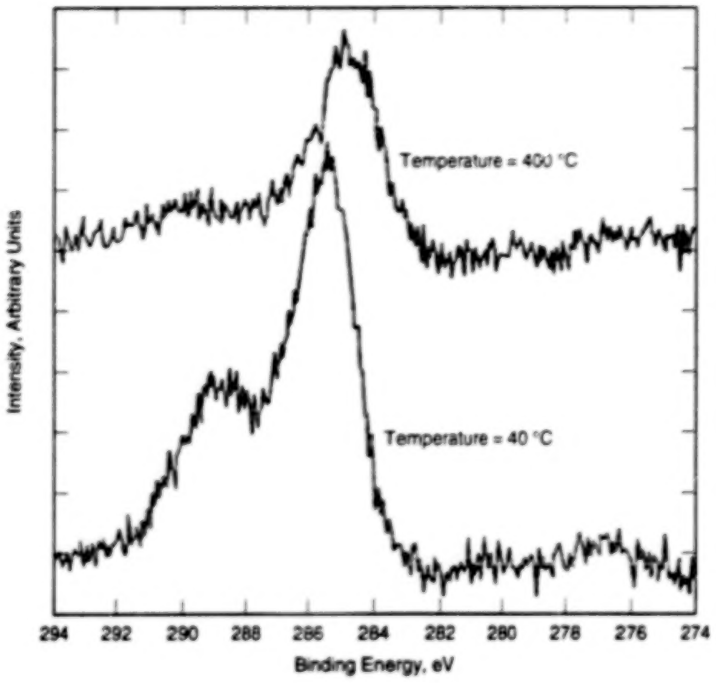

These **X-Ray Photoelectron Spectra** were obtained at the two indicated temperatures during heating of a nickel-alloy specimen that had previously been cleaned by use of methyl ethyl ketone (MEK). These spectra show a decrease in the C(1s) peak, indicative of desorption of carbon in MEK residue.

mens. TGA is practical only for specimens of materials with high surface-area/weight ratios; e.g., materials with fine pores. While XPS is not restricted to any particular range of surface-area/weight ratios, it yields no direct information on adsorption/desorption characteristics.

The prototype TDXPS apparatus was constructed by modifying an XPS system to incorporate a specimen-heating stage and a digital subsystem for feedback control of experiments and acquisition of data. In TDXPS, one acquires x-ray photoelectron spectra at various temperatures as the temperature of the specimen is increased.

TDXPS provides information that cannot be obtained through either technique alone. A succession of two or more spectra at increasing temperatures can be interpreted in terms of a decrease in the concentration of a species of interest (see figure) and/or changes in interactions with other species. Stated somewhat differently, TDXPS yields information about the energy level, reached during the increase in thermal energy of the surface, where each species attains sufficient energy (activation energy) to become desorbed. From activation energies of desorption as determined by TDXPS, one can gain understanding of how surfaces of specific materials become contaminated in various processes. This understanding can be fed back into the designs of processes to decrease or at least beneficially modify contamination.

This work was done by John D. Olivas of Caltech and Enrique Barrera of Rice University for **NASA's Jet Propulsion Laboratory**. *Further information is contained in a TSP [see page 1].*
NPO-20149

Measuring Velocity of Ice by SRI Using Ascending and Descending Passes

Three-dimensional velocity is determined from only two directions.

NASA's Jet Propulsion Laboratory, Pasadena, California

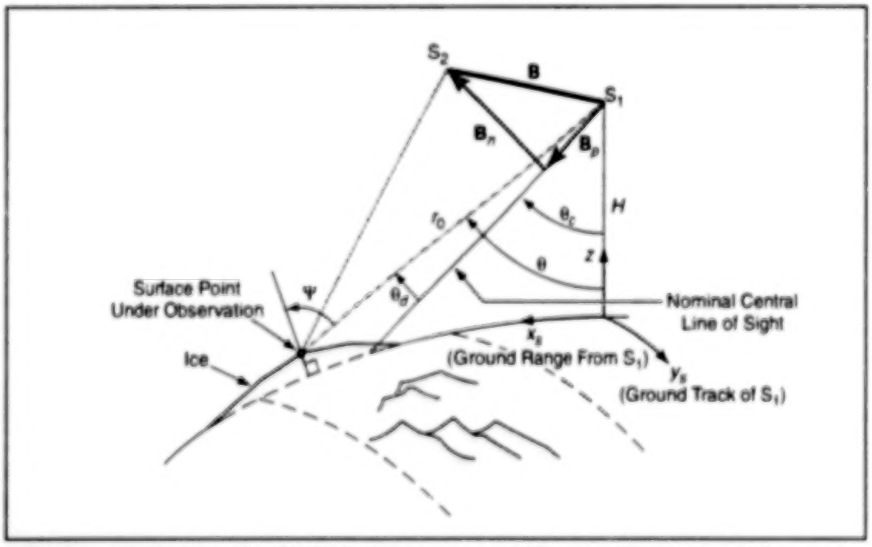

A Point on the Surface of a Glacier Is Observed by a SAR at two different position/time combinations along a nearly repeating trajectory (denoted by S_1 and S_2). The three-dimensional velocity of flow of the ice at the observed point can be estimated from the SAR phase measurements from two crossing orbits, the indicated geometric quantities, and the assumption that ice at the surface flows parallel to the surface.

A method of satellite radar interferometry (SRI) enables the remote measurement of three-dimensional velocities of ice flow over large areas of glaciers. At present, ice-flow velocities are measured primarily *in situ* by use of the Global Positioning System (GPS) in a time-consuming procedure that yields a limited number of data points. In previous efforts to use SRI to determine ice velocities remotely over large areas, measurements were performed along repeat passes. Unfortunately, repeat passes yield data on only the surface displacements associated with the single components of velocity along the radar lines of sight. Moreover, in the absence of additional information, there is no way to separate unambiguously the mixed horizontal and vertical displacement signals acquired via repeat-pass SRI. In contrast, the present method provides

three-dimensional velocity data over large areas with horizontal sampling intervals of roughly 100 m.

In the present method, two sets of repeat-pass measurements are acquired along subsequent, nonparallel passes (one ascending, one descending). The repeat-pass measurement geometry is illustrated in the figure, wherein S_1 and S_2 denotes a synthetic-aperture radar (SAR) viewing the same surface point from two slightly different (near-repeat) positions at different times, and the vector **B** denotes the baseline between the two positions. The problem is to find the vertical component and the two horizontal components of the local displacement of the surface between the two measurement times; the local velocity components then equal these components of displacement divided by the time between acquisition of SAR images.

The basic interferometric quantity is the difference between the relative phases of radar signal returned from the same surface point on the two passes. This phase difference is proportional to the range difference (the difference between the distances along the lines of sight), and can be expressed as a term dependent on displacement plus a term dependent on topography. Provided that the measurement geometry (including **B**) is known, one can estimate the topographical term and thus isolate the displacement-dependent term. For this purpose, **B** is approximated as a linear function of the along-track coordinate, in a mathematical model with four parameters that are determined by a linear least-squares fit to at least four tie points.

Ordinarily, three measurements of the same surface area from three significantly different directions are necessary to measure three-dimensional velocity. However, it is difficult or impossible to acquire such data in the polar regions, where much of the ice of interest is located. In the present method, it is possible to determine all three components of velocity from measurements from only two directions. This is made possible by the assumption that the ice at the surface flows only along the surface. This assumption is somewhat unrealistic in that ice is known to flow slightly upward from the surface in an ablation zone or slightly downward from the surface in an accumulation zone. Nevertheless, the assumption is useful in that it mathematically constrains one component of velocity. The other two components are mathematically constrained by the measurements from the crossing ascending and descending passes. Thus, all three components of velocity are determined.

This work was done by Ian Joughin, Ronald Kwok of Caltech and Mark Fahnestock of the University of Maryland for **NASA's Jet Propulsion Laboratory**. *Further information is contained in a TSP [see page 1].*
NPO-20160

Stereoscopic, Three-Dimensional PIV With Fuzzy Inference

Three-dimensional velocities are measured at points on an illuminated plane of interest.

Lewis Research Center, Cleveland, Ohio

An all-electronic digital particle-image velocimetry (PIV) system has been developed for use in measuring three-dimensional velocities at numerous points throughout a plane of interest in a supersonic flow. This system includes two high-resolution charge-coupled-device (CCD) video cameras oriented for stereoscopic imaging of the plane of interest. Two pulsed neodymium: yttrium aluminum garnet (Nd:YAG) lasers and associated optics illuminate the plane of interest with a sheet of light at two slightly different times to obtain double-exposure images of seed particles entrained in the flow. In principle, the velocity vector represented by the double-exposure image for each particle can be obtained by dividing the interexposure displacement vector by the interexposure time.

In PIV and similar systems described in previous articles in *NASA Tech Briefs*, cameras are aimed perpendicularly to the planes of interest to obtain images indicative of two-dimensional velocities in those planes. Because of the stereoscopy, the images obtained in the present system also contain information on the component of velocity perpendicular to the plane of interest. Of the possible stereoscopic arrangements, the one used in this system involves aiming the lenses of both cameras toward a common point on the plane of interest and tilting the image planes in the cameras to satisfy a condition called the "Scheimpflug condition" (see figure). The advantage of the Scheimpflug condition is that all points of the plane of interest are brought into focus on the image planes, with consequent reduction of the requirement for depth of focus. The Scheimpflug condition entails a minor disadvantage in that it introduces some distortion; for example, a suitably oriented rectangle in the object plane becomes imaged to an isosceles trapezoid. Fortunately, a correction for this distortion can be readily incorporated into the image-data-processing algorithm.

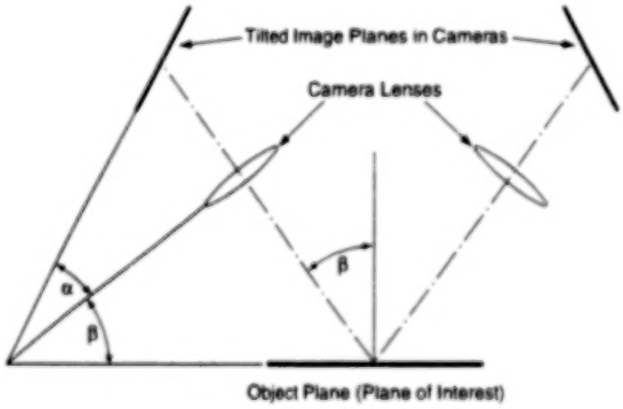

In the **Scheimpflug Condition**, the object plane, the image plane, and the median plane through the lens all intersect at a common point. This condition offers advantages for stereoscopic viewing in the present system, as explained in the text.

The stereoscopic double-exposure images are digitized, the images are divided into regions, and the image data are processed by use of an autocorrelation technique to obtain a candidate-velocity-vector map of the plane of interest.

Typically, this map contains a few erroneous vectors. The most probable candidate velocity vectors are selected in a fuzzy inference operation, in a manner similar to that described in "Digital Particle-Image Velocimetry Enhanced by Fuzzy Logic" (LEW-16415), *NASA Tech Briefs*, Vol. 21, No. 12 (December 1997), page 81. In this operation, the velocity vectors of the five highest correlation peaks (excluding the zero-order peak) in each region are compared with those of the five highest correlation peaks in each of the four surrounding regions. For each region, the velocity vector most similar to the velocity vectors of the selected correlation peaks of the other regions is selected. The justification for selecting velocity vectors on the basis of similarity to adjacent velocity vectors lies in the fundamental continuity of flow.

This work was done by Mark P. Wernet of **Lewis Research Center**. *Further information is contained in a TSP [see page 1].*

Inquiries concerning rights for the commercial use of this invention should be addressed to NASA Lewis Research Center, Commercial Technology Office, Attn: Tech Brief Patent Status, Mail Stop 7-3, 21000 Brookpark Road, Cleveland, Ohio 44135. Refer to LEW-16500.

Endoscopic Shearography Inspection

This nondestructive imaging device allows engineers to detect flaws in closed structures, such as lined fuel tanks.

Marshall Space Flight Center, Alabama

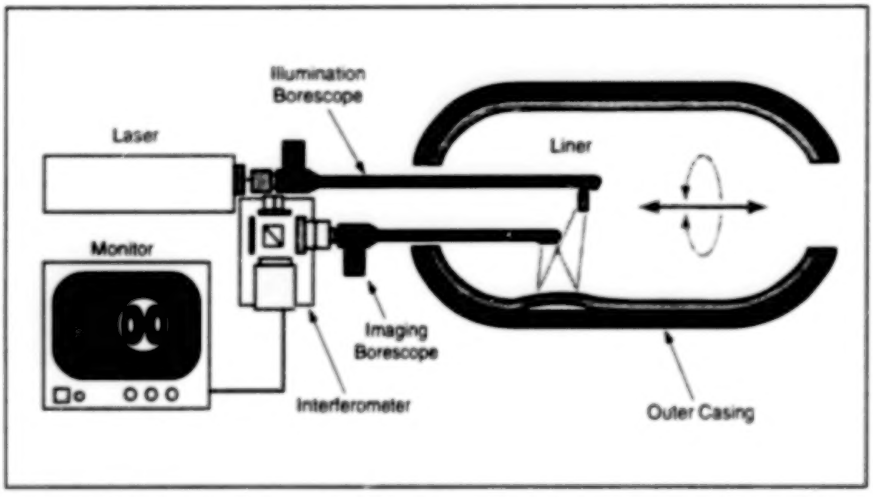

Endoscopic Shearography can detect flaws in composite pressure vessels such as solid-rocket-motor casings.

An imaging method to detect flaws in composite pressure vessels used in the aerospace industry has been developed. Solid-rocket-motor casings and fuel or oxidizer tanks for liquid rocket motors can now be evaluated with the endoscopic shearography inspection device.

The original concept for the endoscopic shearography inspection apparatus was to replace the telephoto zoom lens of a shearography camera with a commercially available borescope. The shearography camera would then be placed outside the test article with the objective end of the borescope inserted through the end boss of the pressure vessel for internal inspection. Either the camera, borescope, or test article would be rotated between inspections to provide full radial or azimuth flaw detection. The camera and borescope or the test article would be translated between inspections to provide full axial detection.

In the final design of the endoscopic shearography inspection device, a pair of borescopes (one for imaging and one for illumination) is positioned parallel to the other. The telephoto lens of a shearography camera was replaced with a side-view rigid borescope. This borescope uses relay lenses and a mirror to image the test article from the objective lens on the borescope tip to the viewing lens of the eyepiece.

In the second borescope, an integrated fiber-optic bundle provides the illumination path, with light entering through the pistol-grip hand and exiting adjacent to the objective lens on the borescope tip. A C-mount adapter was used to provide mechanical stability between the adapter and interferometer, as well as optical coupling of the imaging beam. A gel light guide is used to couple the unexpanded shearography laser beam to the fiber-optic-bundle light guide, which is integrated internal to the borescope.

The unexpanded laser beam enters the eyepiece of the illumination borescope, passes through a series of relay lenses, and is imaged to the borescope objective. The unexpanded laser beam exits the borescope objective and passes through a lens pair, causing the beam to diverge. The distance between the lens-pair elements may be adjusted to increase or decrease the beam divergence to fit the appropriate field of view. The expanding beam illuminates the surface of the test article and is then collected by the objective lens of the imaging borescope. The coherent image passes through a series of relay lenses and is imaged to the borescope eyepiece. The C-mount adapter relays this image to the interferometer for image processing.

Testing of this modified design demonstrated that the endoscopic shearography inspection apparatus with the dual borescopes is able to detect flaws in laminar composite structures.

The demonstrated feasibility of endoscopic shearography suggests that a similar technique can also be used for endoscopic inspections with other nondestructive methods. Thermography, in particular, seems a likely candidate method since it is also an imaging technique often used for the same type of application as shearography.

This work was done by Samuel S. Russell of **Marshall Space Flight Center** *and Matthew D. Lansing of the University of Alabama in Huntsville Research Institute. Further information is contained in a TSP [see page 1].*
MFS-26494

Determining Characteristics of Wind-Borne Particles

Kinetic energies and masses would be computed from impact-acoustic and wind measurements.

NASA's Jet Propulsion Laboratory, Pasadena, California

A small, robust, lightweight, low-power-consumption instrumentation system has been proposed for determining the kinetic energies, masses, and other parameters of wind-borne particles. Originally intended for use in future exploration of Mars, the system might also prove useful on Earth for quantifying the erosive and penetrating characteristics of particles in sandstorms, industrial grit-blasting streams, and the like.

Thin round or square piezoelectric transducer plates with areas between 5 and 10 cm^2 would be mounted on the outside of the instrumentation package, so that they would be exposed to the wind. The impacts of wind-borne particles would emit acoustic signals; that is, they would cause the plates to vibrate. The acoustic signals and the resultant electrical outputs of the transducers would exhibit frequency spectra that would depend primarily on the energies of the impinging particles. (The spectra would also include minor mass-dependent components.)

The leading edge of each transducer output signal in the time domain would serve as a trigger to start analyzing the signal. The analysis would begin with Fourier transformation to convert the time-domain signal to a frequency spectrum. The spectrum would be compared with recorded known spectra to determine the impact energy. In the event that signals representing multiple particle impacts were present during the transformation time, then the system would attempt to decompose the resulting composite spectrum into component spectra associated with the impact energies individual particles.

Impact events can be counted over time to obtain an impact rate. The impact energies computed for events in the count can be used to compute an erosion quotient — a parameter that is useful for quantifying the abrasiveness of impinging dust. If wind-velocity data from ancillary instrumentation were available, and if it were assumed that particles travel at the wind velocity, then the speed and direction of impinging particles, relative to the direction perpendicular to the surface of each transducer could be calculated. The mass of each particle could be calculated from its relative velocity and impact energy. If it were assumed that all particles are of the same density, then the relative sizes of the particles could be determined from their masses. If the density were known, then the absolute sizes could be determined from the masses. One could then also compute a particle-size distribution from the aggregated data on the sizes of the particles included in the count.

This work was done by Frank Hartley of Caltech for **NASA's Jet Propulsion Laboratory**. *Further information is contained in a TSP [see page 1].*
NPO-20221

Electrostatic Dispersion of Fuel Drops To Reduce Soot

A numerical simulation shows that electrostatic dispersion is superior to mechanical dispersion.

NASA's Jet Propulsion Laboratory, Pasadena, California

Electrostatic dispersion of drops of sprayed liquid fuel has been proposed as a technique for reducing the amount of soot formed during burning of the fuel. It is necessary to disperse fuel drops in order to reduce local concentrations of fuel-rich vapors, because such concentrations favor the nucleation of soot. The present technique can be implemented by use of a previously developed device called an "electrostatic triode"; this device puts like electrostatic charges onto sprayed fuel drops to generate dispersion of the drops.

Another technique for reducing the formation of soot is mechanical dispersion through utilization of turbulence. The effectiveness of electrostatic versus mechanical dispersion for reducing the formation of soot has been investigated in a theoretical and computational study. In the study, the mechanical and thermodynamic interactions between fuel drops and the surrounding gases were simulated numerically by use of a mathematical model similar to the models used in previous studies of sprayed liquid fuels that have been performed by the same innovators and summarized in a number of articles in *NASA Tech Briefs*. The model includes, among other conservation equations, equations for the momenta of the drops. The electrostatic forces were included in these equations for those drops that were considered to be charged. The calculations for the charged drops were stopped at the Rayleigh limit; that is, secondary atomization was not modeled.

The results of the numerical simulations were interpreted as signifying that electrostatic dispersion would be superior to mechanical dispersion for reducing the nucleation of soot; this finding gave rise to speculation that perhaps a combination of electrostatic and mechanical dispersion might be even more effective. However, further numerical simulation revealed that for the purpose of reducing the formation of soot, the combination electrostatic and mechanical dispersion would not offer a significant advantage over electrostatic dispersion alone.

This work was done by Josette Bellan and Kenneth Harstad of Caltech for **NASA's Jet Propulsion Laboratory**. *Further information is contained in a TSP [see page 1].*
NPO-20219

Combination of Cryotrapping and SPME for GC/MS Analysis

An improved process has been devised for acquiring and preparing trace amounts of airborne organic compounds for analysis by a gas chromatograph and mass spectrometer (GC/MS). A sample of air is passed through a cryotrap, where organic compounds and water vapor condense on the wall of a tube cooled by liquid nitrogen or dry ice. The condensed material is diluted to a known volume in a sample bottle. An aliquot is taken from the sample bottle. A solid-phase-

microextraction (SPME) fiber (a silica fiber coated with a thin layer of material that adsorbs the organic compounds of interest) is placed in the aliquot to absorb the analyte. The SPME fiber is placed in the injection port of the GC/MS and heated to desorb the analyte onto a cool column. Heretofore, cryotrapping of water has been problematic in sampling for GC/MS, but this process uses cryotrapping of water as an advantage and enables solvent-free injection with minimal preparation of samples. In comparison with older GC/MS sampling processes, this process is faster, utilizes samples more efficiently, and is amenable to sampling of larger volumes of air without concern about water.

This work was done by Dale E. Lueck of **Kennedy Space Center** *and Clyde F. Parrish and Paul H. Gamble of Dynacs Engineering Co., Inc. No further documentation is available.*
KSC-11923

Books and Reports

Evaluation of Droplet-Evaporation Models for Gas/Liquid Flow

A report presents an evaluation of eight mathematical models of the evaporation of liquid droplets — models that are used in the numerical simulation of a variety of gas/liquid flows, including cooling sprays, burning liquid-fuel sprays, fire-suppression sprays, and air/fuel-premixing flows in combustors. Included in the study were two versions of a classical model that includes transient drop-heating effects, four versions of a heat-mass-transfer-analogy model, and two nonequilibrium models based on the Langmuir-Knudsen evaporation law. The models were used to predict evolutions of droplet diameters and temperatures, and the predictions were compared with experimental observations, for droplets of benzene, decane, heptane, hexane, and water vaporizing in convective airflows. All models performed nearly identically at low evaporation rates at gas temperatures significantly lower than the liquid-boiling temperatures. For gas temperatures at and above boiling temperatures, there were large deviations among the various model predictions. Nonequilibrium effects were found to become significant for initial droplet diameters <50 μm, and to increase with slip velocity. The models based on the Langmuir-Knudsen law agreed most closely with the experimental results, though not because they account for nonequilibrium effects; instead, the superiority of these models was attributed to the incorporation of a corrected heat-transfer equation.

This work was done by Josette Bellan, Kenneth Harstad, and Richard Miller of Caltech for **NASA's Jet Propulsion Laboratory**. *To obtain a copy of the report, "Evaluation of Equilibrium and Non-Equilibrium Evaporation Model for Many-Droplet Gas-Liquid Flow Simulations," see TSP's [page 1].*
NPO-20259

Production of Tar in Pyrolysis of Large Biomass Particles

A paper presents a study of the production of tar in the pyrolysis of spherical biomass particles, with computational simulations performed by using the macroparticle portion of the model described in "Generalized Mathematical Model of Pyrolysis of Plant Biomass" (NPO-20068) elsewhere in this issue of *NASA Tech Briefs*. The particles were chosen to have sizes of the order of 1 cm, representative of typical waste wood chips. The numerical results indicate that tar formed in primary reactions decomposes in secondary reactions that occur both within particles and in exterior boundary layers; the net amount of tar available for collection is thereby reduced substantially. An analysis of the competing tar-generation and tar-decomposition reactions results in finding reactor-temperature ranges for maximizing tar yields; the range in a given case is a function of the initial particle size and of the efficiency with which pyrolysis products ejected from particles are cooled and the decomposition reactions thereby quenched in the surrounding medium. The tar yield in a given case also depends on the choice of inert carrier gas, primarily via its effect on the heat capacity of the medium. The report concludes by presenting results of a sensitivity study of the influences of the density, thermal conductivity, and heat capacity of the biomass and of the primary heats of reaction.

This work was done by Josette Bellan and Richard S. Miller of Caltech for **NASA's Jet Propulsion Laboratory**. *To obtain a copy of the paper, "Tar Yield and Collection From the Pyrolysis of Large Biomass Particles," see TSP's [page 1].*
NPO-20067

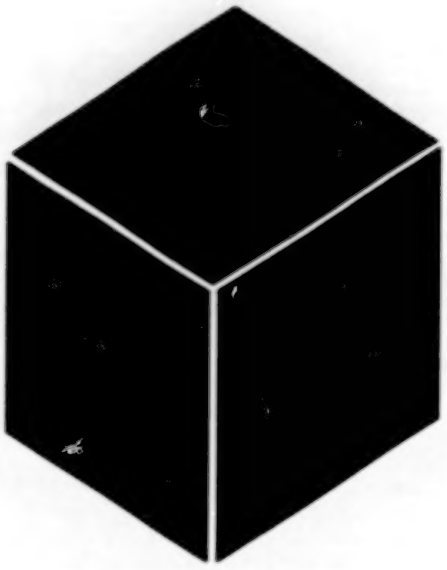

Materials

Hardware, Techniques, and Processes

BLANK PAGE

Improved Nonlinear Mathematical Model of Viscoelasticity

Hereditary integrals are eliminated in an improved rate formulation.

Marshall Space Flight Center, Alabama

An improved nonlinear mathematical model is being developed for use in predicting the complex, time-varying stress-and-strain behaviors of viscoelastic materials. The development of this model is prompted by (1) the lack of success of older constitutive mathematical models that contain hereditary integrals of linear viscoelasticity (e.g., integrals that express current stresses in terms of histories of strains and of relaxation moduli) and (2) the need for a nonlinear model subject to efficient numerical implementation.

A one-dimensional version of the model is given by the equation

$$\sigma(t+\Delta t) = R(\Delta t)\sigma(t) + E_L\int_t^{t+\Delta t}\dot{\varepsilon}(t)dt$$

where $\sigma(t)$ is uniaxial stress, t is the current time, Δt is an increment of time, $R(\Delta t)$ is a relaxation function (which is not the same as a relaxation modulus), E_L is a loading modulus (which is not the same as an initial or tangent modulus), $\varepsilon(t)$ is uniaxial strain, and the overdot signifies differentiation with respect to time. Inasmuch as the time elapsed since initial loading is generally not known in a general-purpose numerical model, it is important that R does not depend on t.

R is defined by applying the equation in the special case of a relaxation test in which ε remains constant for all time. Once R has been defined in this way, E_L is defined by applying the equation to a constant-strain-rate test and rewriting the equation in the following form:

$$E_L = \frac{\sigma(t+\Delta t) - R(\Delta t)\sigma(t)}{\dot{\varepsilon}\Delta t}$$

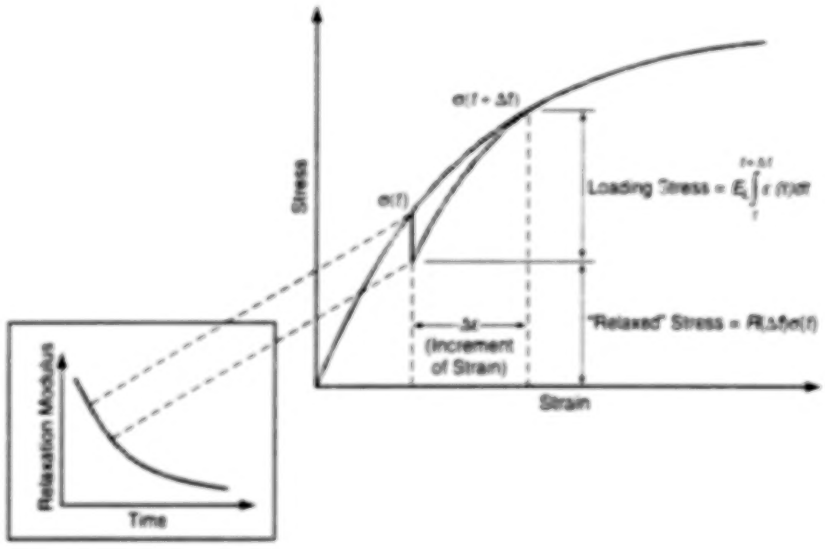

Stress-vs.-Strain Data from a relaxation test are analyzed by use of the model and used to predict the "relaxed" stress in a constant-strain-rate test. The loading modulus is then determined by dividing [the stress measured in a constant-strain-rate test less the "relaxed" stress] by the increment of strain.

Fitting this model to experimental data is expected to be much more straightforward than it is for older nonlinear mathematical models of viscoelasticity; the figure illustrates how this is so. In applying the model, one uses relaxation data to predict relaxation only, and loading data to predict loading.

In general, E_L is expected to be a function of strain, strain rate, temperature, and hydrostatic pressure. R can be approximated conveniently by $R(\Delta t) = \exp(-\Delta t/\alpha)$, where α is a parameter used in fitting the model to experimental data.

Continuing efforts are expected to extend the model to three dimensions and to account for compressibility and dilatation. A tentative three-dimensional model in the form of a tensor rate equation has been proposed.

This work was done by Robert S. Dunham of **Marshall Space Flight Center**. *No further documentation is available.*

Inquiries concerning rights for the commercial use of this invention should be addressed to the Patent Counsel, Marshall Space Flight Center [see page 1]. Refer to MFS-28623.

Computation of Progressive Fracture in a Bolted Laminate

A probabilistic treatment accommodates uncertainties in properties and design variables.

Lewis Research Center, Cleveland, Ohio

A method of computational simulation of progressive fracture in composite-material (matrix/fiber) structural components has been developed. This method does not involve stress-intensity factors or fracture toughnesses. Instead, it involves consideration of the mechanics of the composite from the microscopic (matrix and fiber) constituent level through the subply and ply scales to the structural scale, while using probabilistic techniques to account for uncertainties in such variables as properties of materials, fabrication variables, dimensions, and loads.

The methodology for step-by-step simulation of fracture in a variety of generic composite-material components has been incorporated into the Composite Durability Structural Analysis (CODSTRAN) computer program. CODSTRAN quantifies damage states at all scales except structural by use of the mechanics of composites; the degradation of structural behavior is quantified by use of a finite-element technique in which the damaged part of a structure is treated as not contributing to resistance to load. The

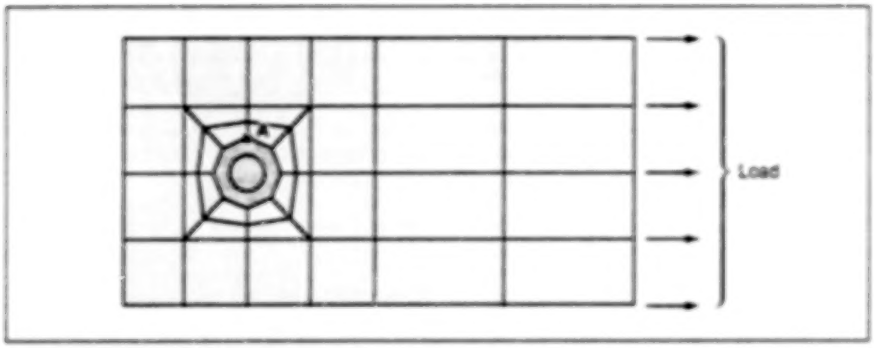

A Composite Panel With a Bolted Joint, subject to an edge load, was represented partly by a finite-element mathematical model. In the computational simulation, damage began at point A.

integration of composite-mechanics and finite-element techniques makes it possible to describe the relationship formally between local conditions (including local damage) and global structural behavior. The criteria for initiation, growth, accumulation, and propagation of damage are examined at each scale and integrated (synthesized) upward through the various scales from microscopic (local) to macroscopic (global). The effects of changes at the global scale (e.g., changes in loading or support conditions) on damage and stress at the local scale are tracked. Overall, global structural equilibrium is maintained by tracking local-to-global and global-to-local effects until convergence is achieved.

The foregoing integrated microscopic-to-macroscopic-mechanics approach is further integrated with the probabilistic approach in the Integrated Probabilistic Assessment of Composite Structures (IPACS) computer program. The resulting overall integrated approach was described previously in "Probabilistic Analysis of Composite-Material Structures" (LEW-16092) *NASA Tech Briefs*, Vol. 21, No. 2 (February 1997), page 58. IPACS starts by defining uncertainties in the properties at the microscopic constituent level. The uncertainties are then propagated to, and combined with, the uncertainties at the next higher scale; that is, subply, then ply, then laminate, then structure (see figure). The uncertainties in the fabrication variables, dimensions, and other variables are carried through the same hierarchy. Consequently, one can obtain probability-density functions (PDFs) and cumulative distribution functions (CDFs) that characterize the responses of structure at all scales from microscopic to macroscopic. One can also obtain sensitivities of structural responses to uncertainties in design variables.

This method has been demonstrated by applying it to a bolted joint in a laminated composite panel under an edge load (see figure). The results showed that the most effective way to reduce end displacement fracture is to control both the load and the ply thickness. The cumulative probability for longitudinal stress in all plies was found to be most sensitive to the load; in the plies with longitudinal fibers, it was very sensitive to ply thickness. The cumulative probability for transverse stress was found to be most sensitive to the coefficient of thermal expansion of the matrix material. The fiber volume ratio and fiber transverse modulus were both found to contribute significantly to the cumulative probability for the transverse stresses in all plies.

This work was done by C. C. Chamis of **Lewis Research Center**; *S. N. Singhal of NYMA, Inc.; and L. Minnetyan of Clarkson University. Further information is contained in a TSP [free page 1].*

Inquiries concerning rights for the commercial use of this invention should be addressed to NASA Lewis Research Center, Commercial Technology Office, Attn: Tech Brief Patent Status, Mail Stop 7–3, 21000 Brookpark Road, Cleveland, Ohio 44135. Refer to LEW-16502.

Regenerable Foam Suppressor

A resin bed eliminates foaming problems during wastewater or electrolysis.

Lyndon B. Johnson Space Center, Houston, Texas

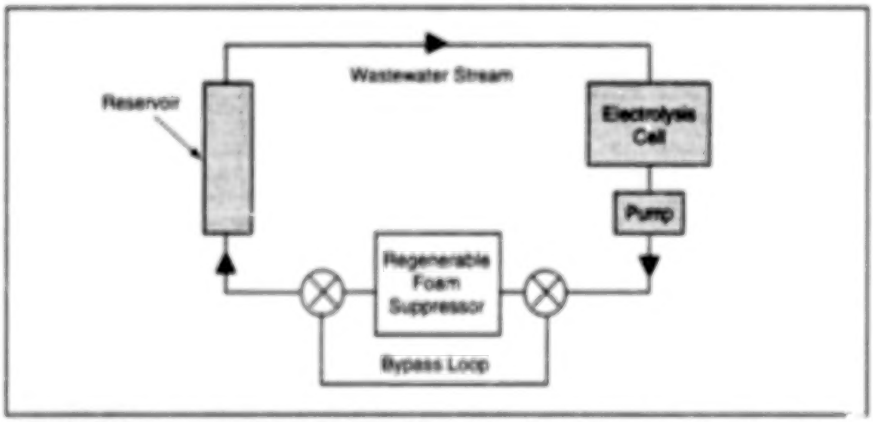

A Resin Bed is incorporated into an electrolytic wastewater-treatment loop to remove foaming agents. When the bed has gone through a cycle of sorption and desorption, the flow is diverted through a bypass loop. The suppressor is compact, occupying only 5 percent of the total volume of the treatment loop.

A foam suppressor removes soap and other foaming agents from a stream of wastewater that is being treated electrolytically. This wastewater is a combination of laundry, hygiene, and urine wastewater. It is desirable to prevent foaming because foaming reduces, by about 15 percent, the efficiency of electrooxidation of waste chemical species. In the absence of foam, the electrochemical sensors used to monitor the treatment process also function more effectively and thus provide more-accurate control of the electrolytic process.

The foam suppressor contains a resin bed that sorbs soaps, detergents, and high-molecular-weight organic compounds with polar or ionic functional groups. Such

materials produce large quantities of foam. Anion-exchange resins are excellent sorbents for such organics: they have large sorption capacities, preferentially sorb foaming agents, and in comparison with activated carbon, are more mechanically stable.

At the beginning of a treatment cycle, the wastewater-treatment loop (see figure) is full of raw wastewater and the electrolysis cell is off. The pump is started and circulates water through the foam suppressor. The resin bed sorbs soap, reducing the concentration of soap in the wastewater. When the concentration of soap in the wastewater becomes insufficient to cause foaming, the electrolysis cell is turned on and begins to oxidize the remaining soap along with the other waste products in the wastewater. As the concentration of soap in the wastewater decreases via electrolysis, the resin bed begins to desorb soap into the wastewater stream. The electrolysis cell oxidizes the soap that reenters the stream. Thus, the bed becomes depleted of soap; that is, regenerated.

When the concentration of soap in the water has fallen to a low value that corresponds to the equilibrium initial concentration in the resin bed, the suppressor is considered to be fully regenerated and is then bypassed. The electrolysis cell continues to operate until the waste organic content of the stream is near zero. At that point, the water is considered to be purified and can be discharged from the loop. The suppressor, with fully restored sorption capacity, is ready for a new batch of soapy wastewater. Beds have operated for 100 such cycles with no loss of foam-suppression ability.

This work was done by James R. Akse and John Thompson of Umpqua Research Co. for **Johnson Space Center**. *Further information is contained in a TSP [see page 1].*
MSC-22299

BLANK PAGE

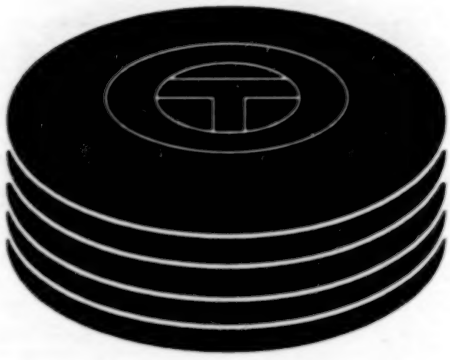

Computer Programs

BLANK PAGE

Computer Programs

These programs may be obtained from COSMIC. Please contact

COSMIC®
Computer Services Annex
University of Georgia
Athens, GA 30602
Telephone No. (404) 542-3265.

Mechanics

Program for Analysis of a Complex Optomechanical System

The IMOS computer program contains subprograms that, collectively, provide a unique capability for multidisciplinary analysis of a system represented by a combination of mathematical models of structural (mechanical), control, thermal, and optical characteristics. One example of such a system would be a telescope equipped with an attitude control subsystem. IMOS enables a user to (1) define the geometry of the system, (2) build a finite-element mathematical model of the system structure, (3) define the system optics in the coordinate system of the finite-element model, (4) add control elements to the model, (5) add mechanical and thermal disturbances to the model, and (6) evaluate the open- and closed-loop performances of the system. IMOS also includes graphical subprograms that enable viewing of structural-assembly operations, structural deformations, and layouts of optical elements. IMOS is written in MATLAB and can be used on any computer that supports MATLAB. The core subprograms are easily coupled in MATLAB, and the user can write additional MATLAB function subprograms. The additional capabilities afforded by the MATLAB control-design, signal-processing, and optimization "toolboxes" enhance the versatility of IMOS. Also included in IMOS are interface subprograms for optical analysis by the MACOS program, thermal analysis by the TRASYS and SINDA programs, and finite-element modeling by the NASTRAN program.

This program was written by Hugh C. Briggs, Daniel Edred, Robert Norton, Andy Kissil, William Ledeboer, Samuel Sirlin, Marie Levine, Jim Melody, Mark Milman, and Laura Needels of Caltech for **NASA's Jet Propulsion Laboratory**. *Further information is contained in a TSP [see page 1].*
NPO-20238

Mathematics and Information Sciences

Quick and Unusually Easy Repository Search Software

Sorting and filtering software tools accelerate searches through large indices.

The Quick and Unusually Easy Repository Search computer program simplifies the search for information contained in a repository of documents at Marshall Space Flight Center. Searching for information on the basis of general subjects can be very time-consuming and frustrating. The repository at Marshall provides an electronic version of an index of documents related to the requester's topic of interest. This index could contain hundreds or even thousands of document titles, index numbers, and NASA contract numbers.

For a researcher equipped with a desktop computer, QUERYS provides the capability to formulate relevant search criteria, reducing the amount of time usually spent narrowing a general subject down to a specific document number. QUERYS converts the repository index into either a Microsoft Access or a Microsoft Excel document. One can then use the robust searching, sorting, and filtering tools of the Microsoft Office software to search through a myriad of document titles to find the documents of interest. Alternatively, one can use Microsoft Word, but its search capability is limited to simple text strings; that is, it does not accommodate filters, sorts, and complex queries. Once a document of interest has been identified by use of QUERYS, one can request a paper copy from the repository.

Written in Microsoft Access Basic and shipped on a 3.5-in. (8.89-cm), 1.44MB MS-DOS diskette, QUERYS can be loaded into any IBM-PC-compatible computer that runs the Windows 95 or Windows NT 4.0 operating system.

This work was done by Michael Neighbors of Sverdrup Technology, Inc., for **Marshall Space Flight Center**. *Further information is contained in a TSP [see page 1].*
MFS-31217

BLANK PAGE

Mechanics

Hardware, Techniques, and Processes

BLANK PAGE

Rigid, Insulating Support for Cryogenic Component

The cryogenic component is suspended on strands that conduct little heat.

Ames Research Center, Moffett Field, California

A structure provides rigid support for a cryogenic component but transmits minimal heat. The structure includes two beams of Invar (or equivalent low-thermal expansion iron/nickel alloy) that are held in alignment, without touching each other, by pretensioned strands of Kevlar® (or equivalent) aromatic polyamide. The strands have a small cross section, low thermal conductivity, high stiffness, and high tensile strength.

The concept of mounting a cryogenic component on thin, low-thermal-conductance tension members is not new; what is new is the particular rigid configuration of this structure, which is illustrated schematically at the top left of the figure. The Invar beams, with their low coefficient of thermal expansion, minimize contraction at low temperatures, which contraction would reduce the tension on the strands and thereby reduce the strength of the support.

As shown in more detail on the bottom part of the figure, the strands are anchored by epoxy in grooves in end plates bolted to the beams; this prevents the weakening effect of knotted or crimped terminations. It also prevents the sudden slackening and consequent loss of tension that can occur when a high tensile load is applied to a strand wrapped in several turns around a terminating shaft or spool.

When a load is applied, for every strand in which the tension increases, there is another strand in which the tension decreases by the same amount. Because increasing tension leads to failure by breakage and the decrease of tension past zero leads to failure by buckling, the structure can be made to support loads over the widest range by pretensioning the strands to about half their breaking strength. (Thus, one ensures that failures in both modes are approached simultaneously.)

The first step in assembling the fixture is to clamp a temporary spacer between the two Invar beams to hold them in alignment. Two strands are rinsed several times in acetone and then dried. The grooves in the end plates are cleaned and roughened by bead blasting, and a small amount of epoxy is applied to them. The assembly is mounted on a lathe between a four-jaw chuck and a live center in the tailstock.

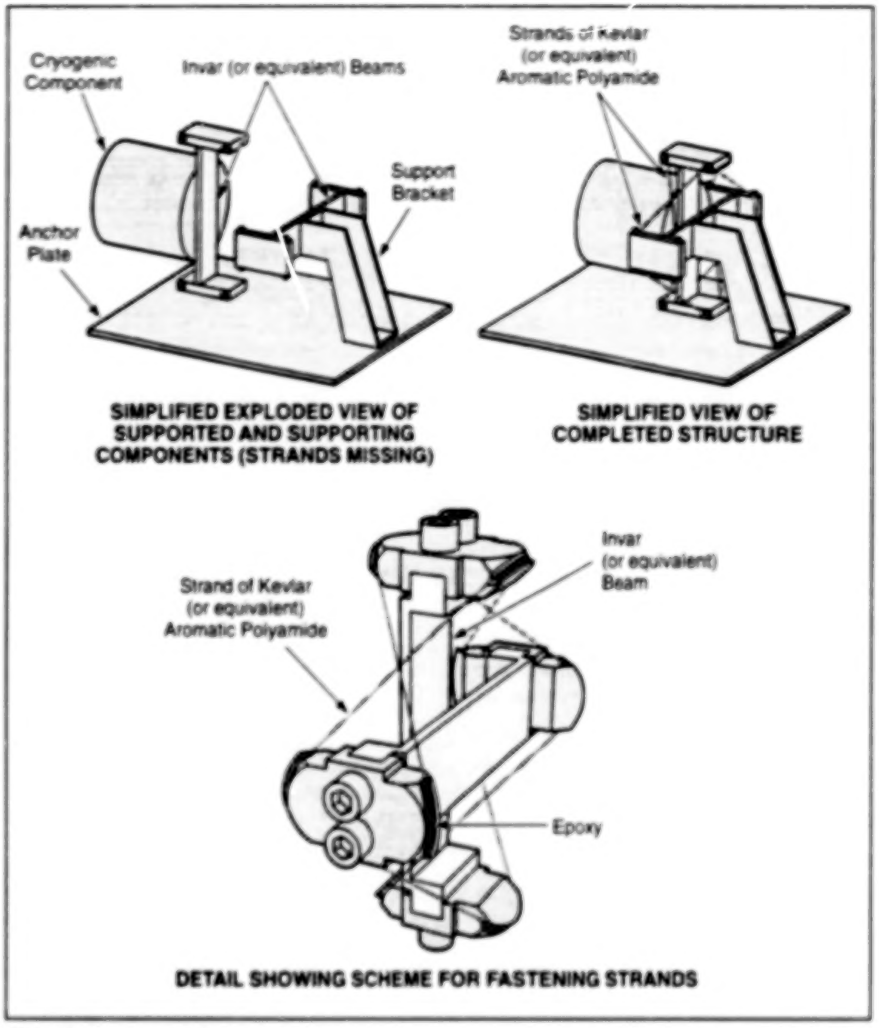

Thin Pretensioned Strands hold Invar beams in alignment, spaced apart from each other to provide a rigid, low-thermal-conductance mount for the cryogenic component.

Each strand is anchored to the fixture, and the fixture is rotated by hand while the strands are guided into the appropriate grooves. The tension is determined by special couplings that slip at a predetermined torque. Before going to the fixture, each strand is wrapped several times around a brass shaft connected to the coupling; the coupling slips and feeds the strand when the correct tension is reached. To prevent the strands from advancing along the shaft as it turns, the shaft has a 15° taper that opposes this tendency. Two slip couplings (one for each strand) are mounted on pivots to allow each strand to be properly positioned as the fixture rotates.

The fixture is wound in multiple rotations so that each link is actually built up of more than one strand. The multistrand approach greatly reduces the stress on the free ends that must be anchored in the epoxy. More epoxy is added to the grooves during winding to cover the strands. The assembly is left under tension until the epoxy hardens. Then the excess lengths of strand are cut off, the assembly is removed from the lathe, and the spacer is removed.

For testing, the fixture was wound with four turns of Kevlar 29 of 50-lb (223-N) breaking strength, which was tensioned to 20 lb (89 N). This resulted in a total cross-section of 0.52 mm^2 and a breaking strength of 200 lb (890 N) for each link. The force and deflection of the fixture were measured at 77 K for an axial compressive load. The reciprocal of axial stiffness was found to be 2.9×10^{-4} in./lb (1.7×10^{-6} m/N). The strands broke at a load of 441 lb (1,962 N).

This work was done by Pat Roach of **Ames Research Center**. *Further information is contained in a TSP [see page 1].*
ARC-11983

Multichannel Ultrasonic-Bolt-Tension-Gauge System

More of the information in the ultrasonic waveform is utilized in a correlation technique.

John F. Kennedy Space Center, Florida

An improved system for measuring tensions in multiple bolts is based on the usual measurement of the times of propagation of ultrasonic waves along the bolts, but the quantities measured and the method of processing the measurement data differ from those of conventional ultrasonic bolt-tension gauges. Typically, a conventional ultrasonic bolt-tension gauge utilizes a single particular feature of the ultrasonic waveform (e.g., a single zero-crossing) to measure the round-trip propagation time. When the gauge is functioning correctly, it can measure time with sufficient accuracy to give the bolt tension within ±2 percent. However, sometimes, the gauge focuses on the wrong signal feature (e.g., the wrong zero-crossing), yielding a reading that can be erroneous by as much as ±30 percent.

The system was initially designed for remote measurement of the tensions in several bolts in an article subjected to a potentially dangerous pressure test. The system includes a commercial ultrasonic bolt gauge with a microprocessor that serves as a gauge controller, plus serial data links between the microprocessor and host computer located in a safe control room remote from the test article. Under control by the computer, the microprocessor causes the ultrasonic bolt gauge to sequentially address ultrasonic transducers on individual bolts and transmit digitized responses to the computer.

Ideally, one would extract maximum information by utilizing the entire ultrasonic waveform rather than only a single feature of the waveform. The approach taken in designing the improved system was to reduce the extent and probability of error by use of a signal-analysis technique, utilizing the full-waveform approach. The improved system implements a correlation technique and also the times of multiple zero-crossings of the ultrasonic waveform for each bolt. The identification of zero-crossings and other signal features is enhanced by use of waveform-feature-recognition software based on three independent mathematical models of bolt gauges. The basic time-interval measurement is obtained from cross-correlating the tensioned and untensioned waveforms. A double- and triple-check is obtained from the zero crossings. If the intervals agree, then the time measured on the waveform for each bolt is considered to be more reliable than if the intervals do not agree. If the intervals do not agree, a vote can be taken and the waveform that does not agree can be discarded. Alternatively, the results can be averaged to obtain a final result that is less erroneous in the worst case.

This work was done by Stuart M. Gleman of I-NET and Lyle J. Robinson, Stephen W. Thayer, Geoffrey K. Rowe, David L. Thompson, and Carl G. Hallberg of Dynacs Engineering Co., Inc., for **Kennedy Space Center**. *Further information is contained in a TSP [see page 1].*

This invention is owned by NASA, and a patent application has been filed. Inquiries concerning nonexclusive or exclusive license for its commercial development should be addressed to the Patent Counsel, Kennedy Space Center; (407) 867-6225. Refer to KSC-11929.

Automated Calibration of Torque Analyzers Without Weights

An automated apparatus calibrates digital torque analyzers that, in turn, are used to verify the accuracies of torque wrenches. The apparatus is located in a central laboratory, and the digital torque analyzers are brought to the laboratory for calibration. Previously, the torque analyzers were calibrated in the field by hanging known dead weights on moment arms of known lengths. That procedure yielded accurate results, but involved transportation and lifting of weights, with risk of injury to technicians. The present apparatus makes it unnecessary to handle weights. Instead, a power jack loads a moment arm via a gearbox and a standard load cell. The apparatus includes a control computer that recognizes the torque analyzer to be calibrated and commands the application of prescribed increments of torque over the range of the torque analyzer. At each increment, the applied torque (calculated from the load-cell reading) is compared with the torque-analyzer reading. When the measurement and comparison have been completed at each increment, the technician presses a button, causing the apparatus to advance to the next increment. When all measurements and comparisons have been completed, the computer prints out the resulting data.

This work was done by Raymond L. Gammon, David W. Kibbey, and Kenneth L. King of United Space Alliance for **Kennedy Space Center**. *Further information is contained in a TSP [see page 1].*
KSC-11986

Machinery

Hardware, Techniques, and Processes

Books and Reports

BLANK PAGE

Making Fuels Onboard for Power Bursts in Exploratory Robots

Products of solar-powered electrolysis would be slowly accumulated for occasional rapid consumption.

NASA's Jet Propulsion Laboratory, Pasadena, California

In-situ resource utilization (ISRU) equipment would be incorporated into remotely controlled exploratory robots, according to a proposal, to generate fuels and oxidizers to extend operational ranges and to provide occasional bursts of power for actions like drilling into the ground, hopping over obstacles, flying, or transmitting data on high-power radio signals. In its original form, the proposal is directed toward the development of a locally refueled planetary explorer (LORPEX) — an exploratory robot that could function on a remote planet, without need for fuel transported from Earth and without need for heavy, bulky power-generating equipment that would be utilized to full capacity only occasionally. The proposal might also be applicable to remotely located scientific instruments (e.g., meteorological instruments) on Earth, or even to automobiles.

The basic idea is that instead of using heavy source that would consume transported fuel to generate high power, one would use a lightweight ISRU unit that would slowly generate a fuel and oxidizer from natural material in its vicinity. The fuel and oxidizer would be stored in lightweight containers (e.g. balloons). The stored fuel could then be consumed rapidly in a lightweight engine or fuel cell to satisfy the occasional demand for high power.

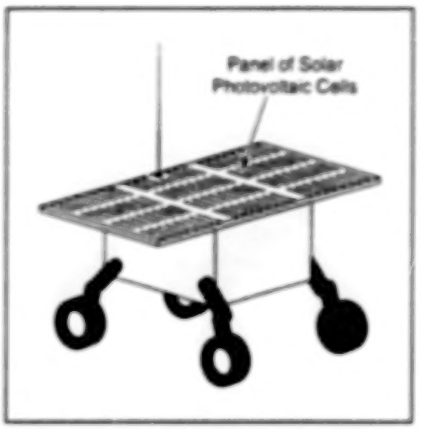

Solar Energy Collected by Photovoltaic Cells would be converted to chemical energy — typically by electrolysis of an oxide to produce a fuel and oxygen.

Typically, a LORPEX and its ISRU unit would be powered by solar photovoltaic cells (see figure). The ISRU unit would generate a fuel and oxidizer through electrolysis. On Earth, Venus, or Mars, for example, one could use a solid-oxide electrolyzer with platinum electrodes to split atmospheric carbon dioxide into carbon monoxide (the fuel in this case) and oxygen. Alternative ISRU units might include SABATIER reactors that would produce hydrocarbon fuels from locally available natural materials; such units might prove useful for enhancing the performances of automobiles.

Two proposals that depart somewhat from the basic ISRU/LORPEX concept offer important potential benefits in terrestrial applications. One of these proposals calls for the use of ISRU units to partly detoxify automotive exhaust by converting CO and CO_2 to O_2 and C. The other proposal calls for sending LORPEX-like robots to hazardous waste sites to detoxify dangerous substances.

This work was done by Kumar Ramohalli of Caltech and Massimiliano Marcozzi of the University of Arizona for **NASA's Jet Propulsion Laboratory**. *Further information is contained in a TSP [see page 1].*
NPO-20269

Solar-Powered Aerobots With Power-Surge Capabilities

Atmospheric gases could be used for energy storage as well as buoyancy control.

NASA's Jet Propulsion Laboratory, Pasadena, California

Advanced aerobots that would be powered by solar photovoltaic batteries and that would be capable of storing energy for occasional operation during short intervals at power levels far beyond those of the photovoltaic batteries have been proposed. Aerobots are robotic balloon-buoyed airborne apparatuses that can be used for exploration of other planets and can be used on Earth for diverse purposes, including monitoring weather, military and law-enforcement surveillance, and entertainment.

The aerobots that have been built thus far utilize various combinations of atmospheric and transported gases for buoyancy control, subject to limitations of available power. The operation of the proposed aerobots would be much less restricted by limitations of available power because they would utilize solar energy and would store excess solar energy in various ways for consumption during such power surges as might be needed for rapid ascents, drilling into the ground, transmitting signals, or other short-term functions.

According to the proposal, part or all of a balloon surface would be covered with solar photovoltaic cells. Detailed calculations show that, with state-of-the-art photovoltaic technology, the mass penalty would be less than 10 percent, since the substrate is already available as the balloon surface. The electric power generated by the cells could be used to electrolyze, compress, liquefy, or freeze a transported or atmospheric gas or to sublimate or boil a frozen or liquid phase of an atmospheric or transported gas. Such physical and chemical manipulations of atmospheric and/or transported gases would be performed to effect changes in buoyancy, to store energy, or to satisfy demands for power surges, depending on circumstances. To cite three examples:

- Products of electrolysis could be stored in canisters or balloon compartments and later consumed in a fuel cell to generate a surge of electric power.
- A compressed gas could be released to provide a rapid change in buoyancy and/or a surge of propulsive force, which could be directed horizontally or could be directed wholly or partly vertically to aid or oppose the change in buoyancy.
- An atmospheric gas could be condensed or frozen to take on ballast, and later allowed to warm up toward ambient temperature to release ballast.

This work was done by Kumar Ramohalli of Caltech for **NASA's Jet Propulsion Laboratory**. *Further information is contained in a TSP [see page 1].*
NPO-20155

Books and Reports

Wheel Drive of Mars Rover

A brief report summarizes the design of the lightweight, high-torque wheel drive of a small robotic vehicle used to explore the surface of Mars. Planetary gearing was selected for compactness and high torque capability. The input stages were fitted with ball bearings to survive the cold (down to −100 °C) Martian atmosphere with very light lubrication. To reduce length, a conventional output shaft and its bearing were not chosen; instead, the last-stage planetary shafts were mounted directly on the wheel hubs. A wheel and its gearing are supported by a single "X"-type main ball bearing that takes radial and axial loads as well as offset moments. The balls in this bearing are made of an acetal plastic and are used without lubrication. To reduce weight, hard-anodized, aluminum races were machined directly into the affected structure; after machining, the races were hard-anodized and coated with polytetrafluoroethylene. The inside diameter of the main bearing is large enough to enable the bearing to contain the motor and gear assembly.

This work was done by Donald B. Bickler, Howard J. Eisen, and Angel Olivera of Caltech for **NASA's Jet Propulsion Laboratory**. *No further documentation is available.*
NPO-20077

Mathematics and Information Sciences

Hardware, Techniques, and Processes

BLANK PAGE

System for Locating Objects of Interest in Image Data Bases

The system is trained from examples.

NASA's Jet Propulsion Laboratory, Pasadena, California

A trainable software system known as JARtool 2.0 has been developed to help scientists find localized objects of interest ("target objects") in image data bases. A human expert implicitly trains the system by using a graphical user interface (see figure) to circle all examples of the target object within a set of images. From the user-provided examples, the system learns an appearance model that can be used to detect the target object in previously unseen images.

JARtool 2.0 is built on top of an image display and graphical user interface program called "SAOtng 1.7," which was developed by the Smithsonian Astrophysics Observatory. JARtool utilizes the basic image labeling and browsing capabilities of SAOtng, but also incorporates components that perform matched filtering, principal components analysis, and supervised classification. These components provide the trainable pattern recognition capability.

In the original application for which it was developed, JARtool has been used to locate small volcanoes in synthetic aperture radar (SAR) images of Venus returned by the *Magellan* spacecraft. However, the system can be applied to other domains. The user must simply supply a new set of training examples for the new class of target objects; there is little or no need for explicit reprogramming.

This work was done by Michael Burl, Usama Fayyad, Padhraic Smyth, Pietro Perona, Saleem Mukhtar, Maureen Burl, Lars Asker, Jayne Aubele, Larry Crumpler, and Joseph Roden for **NASA's Jet Propulsion Laboratory**. *Further information is contained in a TSP [see page 1].*

The **Image** in the display shows a 75 × 75-km region of Venus obtained with synthetic aperture radar by the *Magellan* spacecraft. The JARtool graphical user interface enables the user to develop appearance models of objects of interest and then to apply the models to other images. In this example, the user has started to train the system to locate small volcanoes by circling a volcano in the image.

This software is available for commercial licensing. Please contact Don Hart of the California Institute of Technology at (818) 393-3425. Refer to NPO-20213.

Image Compression for High-Performance Computing

Subband decomposition, vector quantization, and entropy-based encoding are employed in a flexible scheme.

Lewis Research Center, Cleveland, Ohio

A program of research on the use of wavelets for compression of data in a parallel-computing environment has led to development of a scheme for compressing image data. The purpose of the research was to determine whether one could achieve an acceptably high compression ratio with acceptably small loss of image data, at a speed adequate for a given real-time application, provided that one could afford to buy and use any number of modern, high-performance computers in parallel and pipeline processing.

The scheme involves a three-stage pipeline procedure and a "toolkit" of alternative compression methods from which one can choose in customizing the processing for a given application. In the first stage in the pipeline, no compression takes place; instead, the data are processed through filters defined by the user to decompose the data into subbands (e.g., frequency or wavelet subbands) in preparation for the subsequent stages.

In the second stage, the data in each subband are compressed by use of vector quantization. As in any quantization method, some information is lost. Because vector quantization is computationally demanding, it is accomplished by use of multiple high-performance computers in a parallel-processing, message-passing architecture.

In the third stage, compression is effected by a method of entropy-based encod-

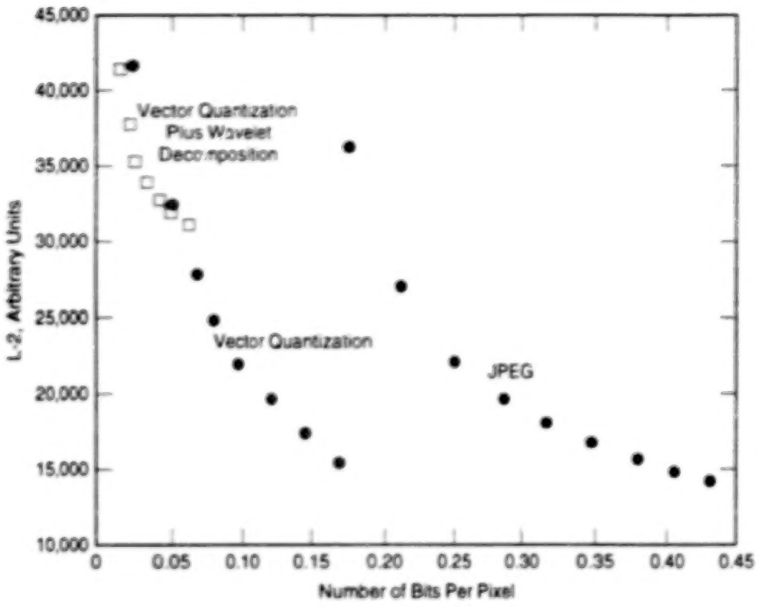

This **Plot of Data From a Computational Experiment** on a test image illustrates the superiority of the wavelet-decomposition/vector-quantization version of the present scheme over the JPEG scheme in terms of the L-2 metric, which is the sum of squares of errors between original and reconstructed (final decoded) versions of the pixels in the image.

ing. The encoding in this stage is lossless and can result in doubling of the compression ratio with little or no increase in computational complexity.

Computational experiments were performed to test two versions of the present scheme in comparison with each other and with the Joint Photographic Experts Group (JPEG) scheme, which is a lossy scheme particularly useful for compression of color image data with little apparent image degradation as perceived by the human eye. One version of the present scheme included vector quantization with subband (wavelet) decomposition; the other version included vector quantization without subband decomposition. The primary findings from the experiments are that (1) vector quantization is the major source of compression and (2) by use of wavelet-based subband decomposition, one can increase the compression ratio, albeit with a concomitant increase in the error rate. The performance of the present scheme was found to be superior or at least equal to that of the JPEG scheme in the test cases (see figure).

This work was done by Harry Barryman, James Navern, Jr., and Gary Davison of Ronin Systems, Inc., and Manos Papaefthymiou for **Lewis Research Center**. *Further information is contained in a TSP [see page 1].*

Inquiries concerning rights for the commercial use of this invention should be addressed to NASA Lewis Research Center, Commercial Technology Office, Attn: Tech Brief Patent Status, Mail Stop 7–3, 21000 Brookpark Road, Cleveland, Ohio 44135. Refer to LEW-16372.

National Aeronautics and
Space Administration

END

02\09\99